Cell Stem Cell

Article

Self-organization of mouse embryonic stem cells into reproducible pre-gastrulation embryo models via CRISPRa programming

Graphical abstract

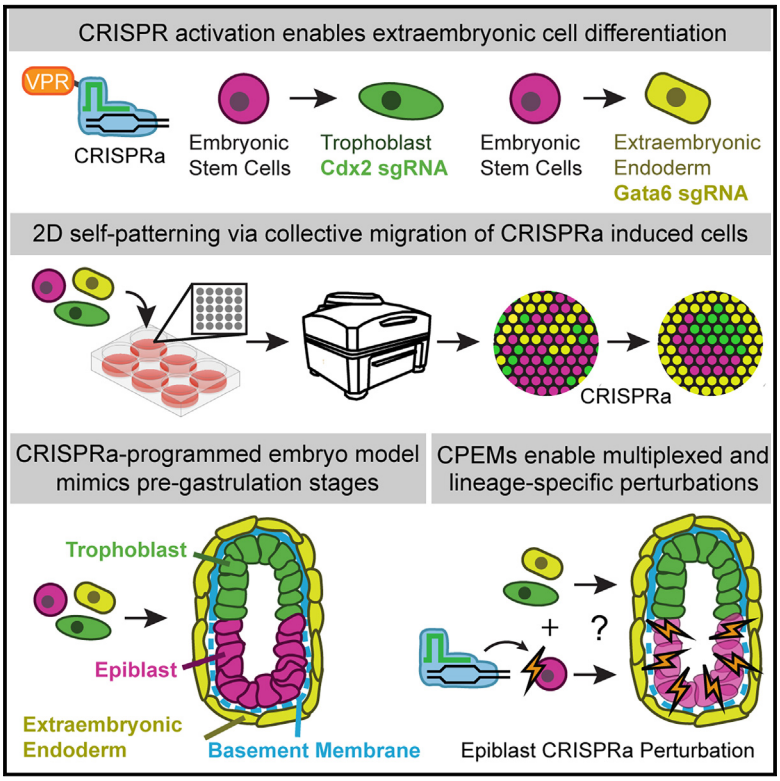

Highlights

- CRISPR activation enables efficient mouse extraembryonic lineage differentiation
- CRISPRa-programmed embryo models (CPEMs) mimic the pre-gastrulation embryonic stage
- Self-patterning emerges via the collective migration of CRISPRa-programmed cells
- CPEMs enable multiplexed, lineage-specific perturbations to study morphogenesis

Authors

Gerrald A. Lodewijk, Sayaka Kozuki, Clara J. Han, ..., Randolph Ashton, Lei S. Qi, S. Ali Shariati

Correspondence

alish@ucsc.edu

In brief

Lodewijk et al. develop a CRISPRa-programmed embryo model using mouse pluripotent cells. By introducing controllable CRISPR activation tools into pluripotent cells, they enabled the efficient generation of a reproducible model. These tools were also used to disrupt developmental pathways, offering a method to study mechanisms of developmental disorders.

Lodewijk et al., 2025, Cell Stem Cell *32*, 1–19
June 5, 2025
https://doi.org/10.1016/j.stem.2025.02.015

CellPress

Cell Stem Cell

CellPress
OPEN ACCESS

Article

Self-organization of mouse embryonic stem cells into reproducible pre-gastrulation embryo models via CRISPRa programming

Gerrald A. Lodewijk,[1,2,3,11] Sayaka Kozuki,[1,2,3,11] Clara J. Han,[1,2,3] Benjamin R. Topacio,[1,2,3] Seungho Lee,[1,2,3] Lily Nixon,[1,2,3] Abolfazl Zargari,[4] Gavin Knight,[5,6] Randolph Ashton,[5,6,7] Lei S. Qi,[8,9,10] and S. Ali Shariati[1,2,3,12,*]

[1]Department of Biomolecular Engineering, University of California, Santa Cruz, Santa Cruz, CA, USA
[2]Genomics Institute, University of California, Santa Cruz, Santa Cruz, CA, USA
[3]Institute for The Biology of Stem Cells, University of California, Santa Cruz, Santa Cruz, CA, USA
[4]Department of Electrical and Computer Engineering, University of California, Santa Cruz, Santa Cruz, CA, USA
[5]Neurosetta LLC, Madison, WI, USA
[6]Wisconsin Institute for Discovery, Madison, WI, USA
[7]Department of Biomedical Engineering, University of Wisconsin-Madison, Madison, WI, USA
[8]Department of Bioengineering, Stanford University, Stanford, CA, USA
[9]Sarafan ChEM-H, Stanford University, Stanford, CA, USA
[10]Chan Zuckerberg Biohub, San Francisco, San Francisco, CA, USA
[11]These authors contributed equally
[12]Lead contact
*Correspondence: alish@ucsc.edu
https://doi.org/10.1016/j.stem.2025.02.015

SUMMARY

Embryonic stem cells (ESCs) can self-organize into structures with spatial and molecular similarities to natural embryos. During development, embryonic and extraembryonic cells differentiate through activation of endogenous regulatory elements while co-developing via cell-cell interactions. However, engineering regulatory elements to self-organize ESCs into embryo models remains underexplored. Here, we demonstrate that CRISPR activation (CRISPRa) of two regulatory elements near Gata6 and Cdx2 generates embryonic patterns resembling pre-gastrulation mouse embryos. Live single-cell imaging revealed that self-patterning occurs through orchestrated collective movement driven by cell-intrinsic fate induction. In 3D, CRISPRa-programmed embryo models (CPEMs) exhibit morphological and transcriptomic similarity to pre-gastrulation mouse embryos. CPEMs allow versatile perturbations, including dual Cdx2-Elf5 activation to enhance trophoblast differentiation and lineage-specific activation of laminin and matrix metalloproteinases, uncovering their roles in basement membrane remodeling and embryo model morphology. Our findings demonstrate that minimal intrinsic epigenome editing can self-organize ESCs into programmable pre-gastrulation embryo models with robust lineage-specific perturbation capabilities.

INTRODUCTION

New frontiers are emerging in the study of mammalian embryogenesis through engineering stem cell-based embryo models (SEMs) using the unrestricted potential of embryonic stem cells (ESCs) and their self-organizing behavior.[1–26] SEMs can reproduce key aspects of spatial organization of pre- and post-gastrulation stages of embryonic development with potential to implant[1,23,24,27] or advance to later stages of development.[2,3] SEMs can be generated through self-assembly of mouse ESCs (mESCs) with extraembryonic cells. For example, preimplantation blastocyst-like structures are formed by assembling mouse trophoblast stem cells (TSCs) with mESCs, recapitulating the organization and transcriptional programs of natural blastocysts.[1,4] Similarly, post-implantation embryo-like models can be generated by assembling mESCs with TSCs and extraembryonic endoderm-like (XEN) cells, exhibiting hallmarks of post-implantation embryos, including the establishment of anterior signaling centers.[5,28,29] SEMs can also leverage the self-patterning capacity of mESCs to form ordered structures in response to biochemical and biomechanical cues. Earlier work shows aggregates of mESCs can form posterior domains and symmetry breaking in response to activation of Wingless-Type MMTV Integration Site (Wnt) signaling.[10] Recently, it was shown that mESC aggregates exposed to pulses of Wnt can undergo gastrulation-like events, forming gastruloids that replicate the body axis formation and spatiotemporal gene expression patterns of natural embryos.[9,23] The self-patterning capabilities of ESCs are conserved across species, enabling the generation of human embryo-like structures.[12,14,16,17,19,21–24,30,31] SEMs

Please cite this article in press as: Lodewijk et al., Self-organization of mouse embryonic stem cells into reproducible pre-gastrulation embryo models via CRISPRa programming, Cell Stem Cell (2025), https://doi.org/10.1016/j.stem.2025.02.015

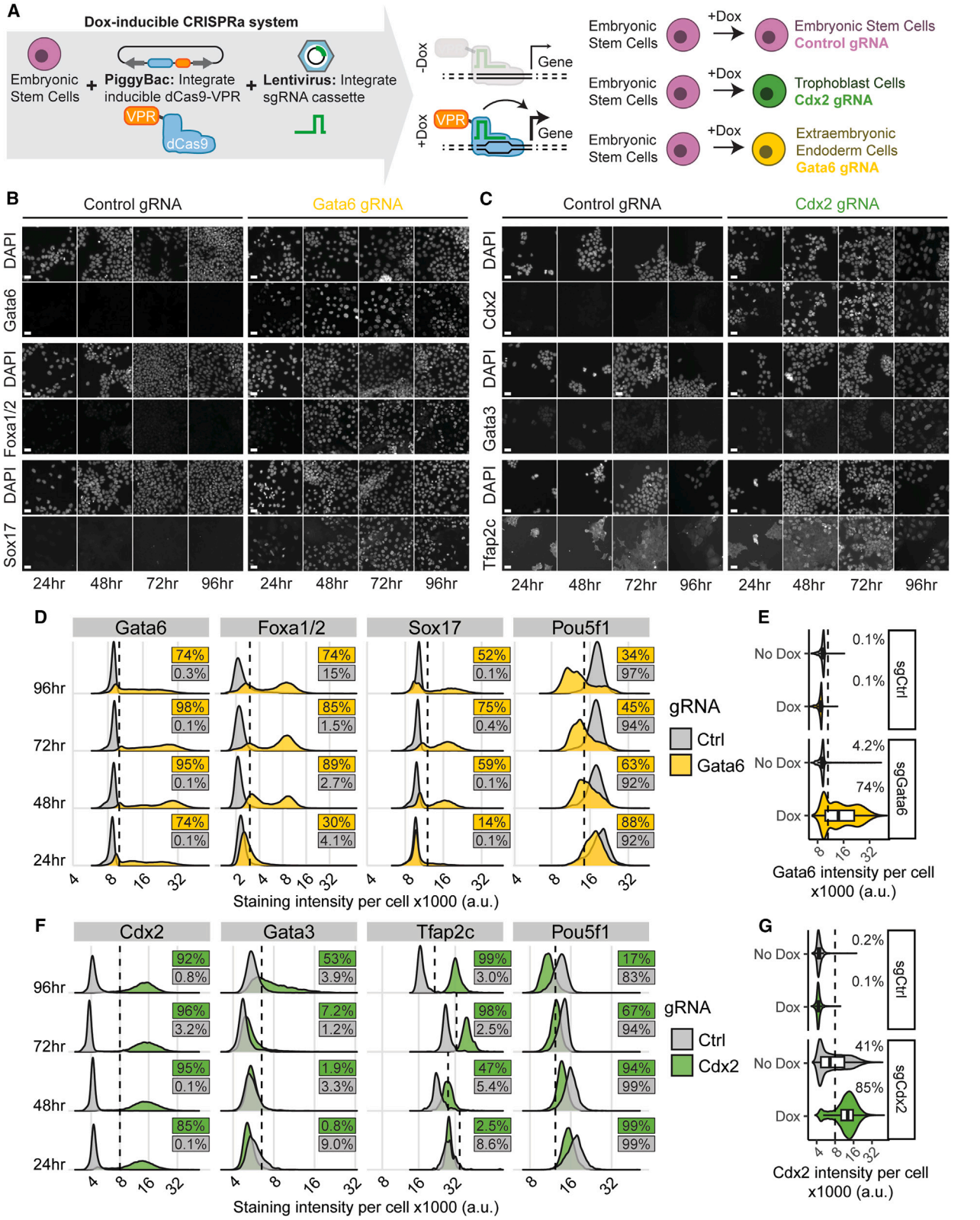

Figure 1. Design and validation of doxycycline-inducible CRISPRa mESCs

(A) Overview of CRISPRa cell system.

(B) Time-course immunofluorescence staining of Gata6, Foxa1/2, and Sox17 in sgGata6-mESCs treated with doxycycline up to 4 days.

(legend continued on next page)

have the potential to offer transformative insights into principles of self-organization in early embryogenesis and the origins of developmental abnormalities.

Current methods for the generation of SEMs rely on combinations of the following: (1) biochemical optimization of media with lineage-specific morphogens or small molecules[8,13,16,19,23] and (2) exogenous overexpression of transcription factors.[2,14,28,32,33] Recent reports have used a combination of transcription factor-induced cell types and natural embryo-derived cell lines to create embryo models, enabling the study of key processes like lumen formation and the initiation of gastrulation.[2,3,28,29,32] During embryogenesis, however, epigenetic changes in the endogenous regulatory elements of cell-fate-determining factors drive the differentiation of specialized cell types that co-develop into an embryo. We hypothesized that epigenetic recapitulation of endogenous regulatory elements of such factors is sufficient to form major cell types of the embryo and self-organize them into embryo-like structures. By leveraging the programmability of CRISPR activation (CRISPRa) tools, we showed that activation of just two endogenous non-coding regulatory elements near Cdx2 and Gata6 genes is sufficient to self-organize mESCs into embryo-like structures with morphological features reminiscent of the days 5 to 6 mouse embryo. We present a straightforward approach to generate highly consistent mouse embryo models through intrinsic epigenetic control and without dependency on externally added lineage-specific signaling factors. CRISPRa-programmed embryo models (CPEMs) form within 3 days in a simple medium with nutrients and serum, only through chemical induction of CRISPRa. We use single-cell timelapse microscopy to reveal collective cellular motion that results in the formation of embryonic patterns. Single-cell transcriptome analysis of CPEMs showed emergence of embryonic cell types expressing markers of each lineage while capturing known and potential new cell-cell signaling pathways. Using the multiplexing potential of CRISPRa, we show that simultaneous activation of Elf5 and Cdx2 enhances the differentiation of TSCs and their integration into CPEMs. CPEMs exhibit asymmetry along their major axes with spatial cellular arrangement similar to pre-gastrulation natural embryos (E5.5), with a subset forming anterior visceral endoderm (AVE)-like regions. Importantly, we demonstrate that CRISPRa enables precise, lineage-specific activation of large, complex genes—such as the 120 kb laminin gene—and their associated matrix metalloproteinases (Mmp) to investigate roles of basement membrane (BM) remodeling and embryo shape formation, highlighting a key application for CPEMs for gene perturbation experiments. In sum, we propose a CRISPRa-based method to self-organize ESCs into pre-gastrulation mouse embryo models with highly consistent spatial organization that allows for rapid interventional experiments without requiring external lineage-specific signaling cues.

RESULTS

Generation of CRISPRa-induced XEN cells and trophoblast cells

Exogenous overexpression of coding sequences of cell-fate-determining transcription factors has been widely used for controlled differentiation or reprogramming of cells. However, chromatin context, presence of co-factors, excessive expression level, and epigenetic barriers can limit the activity of exogenous transcription factors. Additionally, induced transcription factors often bypass post-transcriptional RNA splicing, a widespread process with critical functional implications for transcription factors.[34] Thus, we leveraged CRISPRa to induce cell-fate-determining transcription factors using their native regulatory elements. We hypothesized that direct CRISPRa of endogenous regulatory elements can overcome epigenetic barriers associated with differentiation of ESCs.[35–38] To test our hypothesis, we implemented a CRISPRa-based strategy to generate cell types that comprise the mouse peri-implantation embryo: epiblast stem cells (Epi), TSCs, and XEN cells. We generated a doxycycline-inducible CRISPRa ESC line to activate regulatory elements of two major cell-fate-determining transcription factors, Cdx2 (sgCdx2-mESCs) and Gata6 (sgGata6-mESCs), that are expressed in TSCs and XEN cells, respectively.[2,39–44] As a control, we used mESCs expressing a non-targeting control single guide RNA (sgRNA) (sgCtrl-mESCs) (Figure 1A). We designed our sgRNAs to recruit CRISPRa to proximal regulatory elements of Gata6 and Cdx2 that show increased chromatin accessibility during natural development of XEN and TSCs in mouse embryos observed in previously published data[45,46] (Figure S1A). 24 h after induction of CRISPRa in sgGata6-mESCs, we observed a robust and specific expression of Gata6 (Figure 1B). Similarly, we were able to observe Cdx2 expression via induction of CRISPRa in sgCdx2-mESCs (Figure 1C). Induction of Gata6 was found in 90% of cells and followed by expression of additional markers of XEN cells, Foxa1/2 and Sox17, and a rapid reduction in Pou5f1(Oct4), a marker of pluripotency (Figure 1D). In sgCtrl-mESCs or sgGata6-mESCs without doxycycline treatment, we did not observe major increases in Gata6 expression and downstream markers, Foxa1/2 and Sox17, or a decrease of the pluripotency factor Pou5f1 (Figures 1E and S1B). Like sgGata6-mESCs, we observed robust and specific expression of Cdx2 in sgCdx2-mESCs 24 h after induction of CRISPRa, which was not the case for sgCtrl-mESCs (Figure 1F). Induction of Cdx2 was found in more than 90% of cells and was followed by upregulation of additional TSC lineage markers, Tfap2c and Gata3, at days 3 and 4, respectively, while Pou5f1(Oct4) gradually declined at day 4 (Figures 1F and S1C). We observed expression of Cdx2 in a percentage of sgCdx2-mESCs in the absence of doxycycline, likely because of minimal leakiness of tet-responsive elements, a known limitation of inducible systems.[47] However, this background expression was not sufficient to

(C) Time-course immunofluorescence staining of Cdx2, Gata3, and Tfap2c in sgCdx2-mESCs treated with doxycycline for 4 days.
(D) Quantification of Gata6 induction and related XEN-cell markers over time.
(E) Comparison of Gata6 induction in sgCtrl- and sgGata6-mESCs treated with or without dox.
(F) Quantification of Cdx2 induction and related TSC markers over time.
(G) Comparison of Cdx2 induction in sgCtrl- and sgCdx2-mESCs treated with or without dox. Plots show collective distribution of cells from 16 images each per condition with at least two experimental replicates. All scale bars indicate 40 μm.

Please cite this article in press as: Lodewijk et al., Self-organization of mouse embryonic stem cells into reproducible pre-gastrulation embryo models via CRISPRa programming, Cell Stem Cell (2025), https://doi.org/10.1016/j.stem.2025.02.015

induce expression of mature TSC lineage markers, Tfap2c and Gata3, or to decrease Oct4 expression to the same extent as the dox-treated conditions (Figures 1G and S1C). After 48–72 h of induction, a majority of dox-treated cells show double-positive-staining Gata6 and Foxa1/2 or Sox17 in the sgGata6-mESCs, and double-positive-staining for Cdx2 and Tfap2c in the sgCdx2-mESCs (Figures S1D, S2A, and S2B). These findings show that CRISPRa-mediated epigenome activation efficiently generates major extraembryonic cell types in a simple medium with nutrients and serum, without the need for external lineage-specific signaling cues or exogenous transcription factors.

CRISPRa of two regulatory elements can self-organize ESCs into 2D embryonic patterns

Changes in endogenous regulatory element activity are linked to embryonic cell differentiation and spatial patterning. We hypothesized that activating key developmental regulatory elements can form spatially ordered patterns. To test this, we plated sgGata6-mESCs, sgCdx2-mESCs, and sgCtrl-mESCs together on circular micropatterns to form colonies with reproducible sizes[15,48] followed by induction of CRISPRa for 72 h (Figure 2A). The simplicity of the 2D micropattern system allows for studying dynamics of cellular motions for specific lineages, self-patterning, and cellular interactions without the complexity and measurement challenges of a 3D model. Next, we stained for Foxa1/2 to detect CRISPRa-induced sgGata6-mESCs, Cdx2 to detect CRISPRa-induced sgCdx2-mESCs, and Pou5f1(Oct4) to detect sgCtrl-mESCs. CRISPRa-induced cells on circular micropatterns formed ordered structures where sgGata6-mESCs (Foxa1/2+) frequently formed a ring-like structure around the colony while sgCdx2-induced cells (Cdx2+) were clustered inside the colony adjacent to sgCtrl-mESCs (Pou5f1+) (Figures 2B and S3A). This organization is reminiscent of the XEN lineage encircling the epiblast and extraembryonic ectoderm in natural peri-implantation embryos, highlighting the potential of 2D micropatterns to capture aspects of embryonic spatial patterning.[44,49] Interestingly, emergence of spatially ordered 2D patterns depends on the colony size. Smaller colonies with 80 or 140 μm diameters more consistently formed ring-like structures, but larger colonies with 225 or 500 μm diameters did not form similar patterns upon induction of CRISPRa (Figures 2B, 2C, and S3A–S3D). None of these patterns emerged without doxycycline (Figures S3E–S3H). This suggests that in confined 2D micropatterns, the scaling of embryonic self-patterning formation can be limited by effectiveness of short-range biochemical or biophysical interactions, overall growth area, and cellular composition. Analysis of cell number and ratio in micropatterned discs of different sizes showed that loss of patterning is correlated with an increased number and ratio of Pou5f1+ cells, whereas we observed a decreased number and ratio of Foxa1/2+ and Cdx2+ cells as the diameter of the colony increases (Figures 2D, 2E, and S3I). We also observe more variation in cell ratios at the lower density regions, likely due to stochastic effects of few cells initially populating these regions, as observed in quantification of individual regions (Figure S3I), suggesting that in some cases, the smallest micropattern regions are seeded by just 1 or 2 cell types. Despite starting out with an equal ratio of cells in each region size at the seeding time, in the smaller 80 and 140 μm colonies, the Pou5f1+ population is likely restricted by overall growth area due to geometrical confinement, while in the larger 225 and 500 μm regions, the expanded growth area allows for additional cell division without being restricted by space or neighboring cells. These results show that direct CRISPRa of two regulatory elements in ESCs promotes differentiation and formation of 2D spatially organized peri-implantation-like patterns intrinsically without addition of lineage-specific external morphogens or chemicals. Self-patterning through intrinsic CRISPRa induction of cell fate depends on micropattern size, which determines the overall colony size and cellular composition of embryonic structures.

Collective motion of proliferating cells results in self-patterning

How do spatially ordered embryonic patterns emerge from a few randomly positioned individual cells? To answer this, we used the uniform circular morphology of CRISPRa-programmed 2D embryonic patterns to track cells and examine cellular motion and spatial organization with single-cell live fluorescent imaging. To visualize each CRISPRa-induced cell type, we designed constructs in which sgCdx2 is co-expressed with Clover-nuclear localization signal (NLS) and sgGata6 is co-expressed with mCherry-NLS, resulting in sgRNA and fluorescent protein expression from the same construct (Figure 3A), allowing us to monitor each cell type in real time. We verified that Clover-NLS (sgCdx2) and mCherry-NLS (sgGata6) signals overlap with Cdx2 and Gata6 staining, respectively, by using live imaging followed by endpoint staining for the corresponding markers (Figures S3J and S3K). After seeding cells on RosetteArray well plates[50] with 100 μm micropatterned regions, we imaged in 1 h intervals for 48 h for both doxycycline-treated cells and controls without doxycycline (Figure 3A). We imaged regions with all three cell types present and via single-cell segmentation and tracking monitored dynamics of pattern formation. Initially, there were no discernible cellular motion patterns. However, we observed noticeable differences in patterns of cellular motions of CRISPRa-induced cells in later time points. CRISPRa-induced sgCdx2-mESCs cells self-assemble into clusters moving toward each other over time (Figure 3B; Video S1A). On the other hand, sgGata6-mESCs cells displayed cooperative behavior by gradually moving to the edges of the micropatterns, which was followed by a collective rotational movement to form a ring around other cells[51–55] (Figure 3B; Videos S1A and S1B). Non-doxycycline control cells moved randomly and lacked a specific pattern, as shown by the interspersed Clover and mCherry signals (Figure 3C). At the start, we noticed that pattern formation begins with just a few (4–8) CRISPRa-induced sgGata6-mESCs and sgCdx2-mESCs that proliferate, but CRISPRa-induced sgCdx2-mESCs displayed a decreased cell number toward the end of the 48-h experiment, when compared with CRISPRa-induced sgGata6-mESCs or to no dox treatment (Figure 3D). Accordingly, we observed an increase in the cell cycle duration for sgCdx2-mESCs compared with sgGata6-mESCs treated with dox (Figure 3E). To test if pattern formation is paired with directionality, we quantified the angular movement of cells relative to the center of micropattern regions. The results show that CRISPRa-induced cells display different patterns of angular movements over time when compared with non-induced sgGata6-mESCs and sgCdx2-mESCs, which was more pronounced for sgGata6-mESCs (Figures 3F, S3L, and S3M). To

Please cite this article in press as: Lodewijk et al., Self-organization of mouse embryonic stem cells into reproducible pre-gastrulation embryo models via CRISPRa programming, Cell Stem Cell (2025), https://doi.org/10.1016/j.stem.2025.02.015

CellPress
OPEN ACCESS

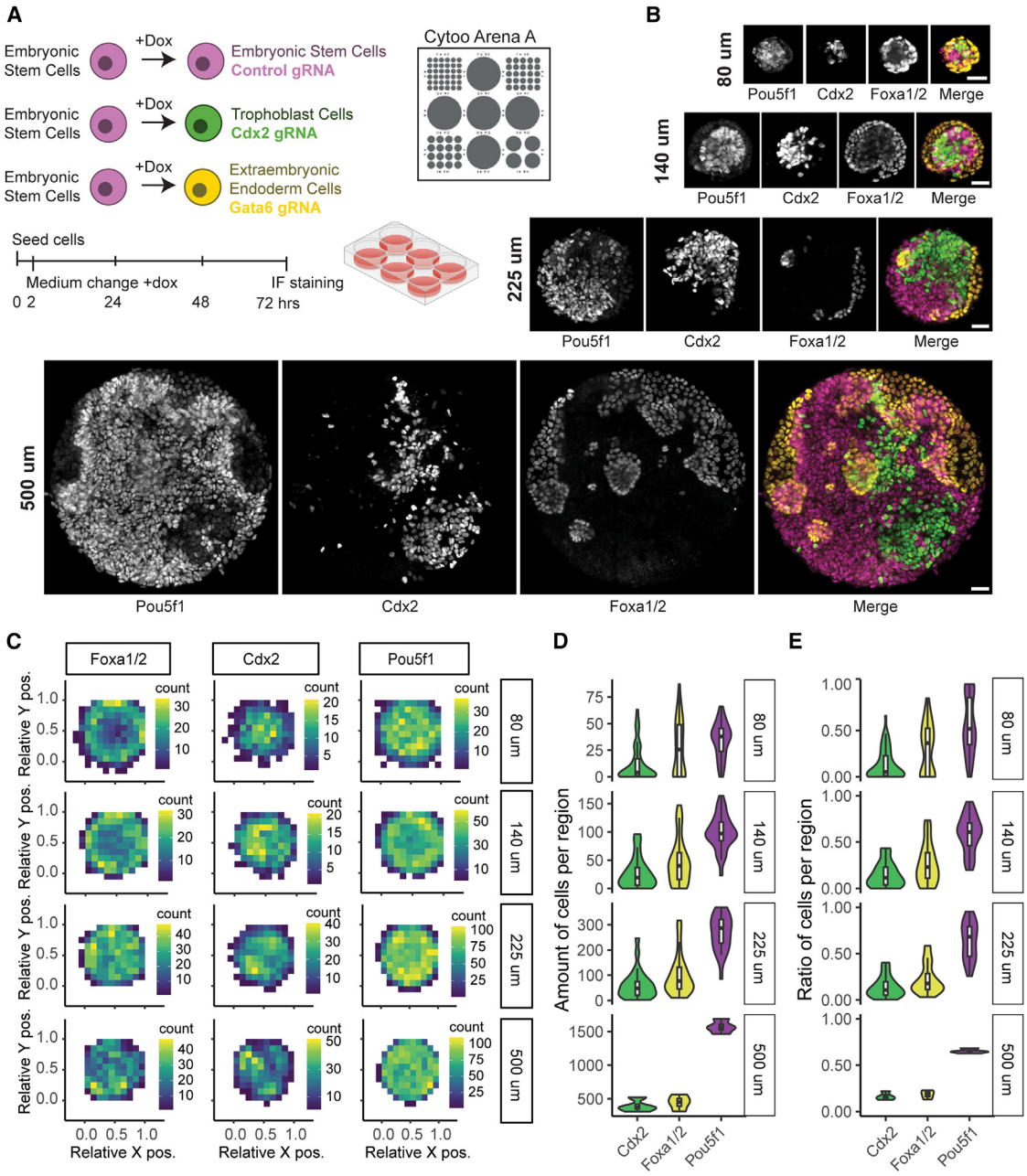

Figure 2. 2D micropattern organization of sgCtrl-, sgCdx2-, and sgGata6-induced mESCs

(A) Overview of cells and protocol used on micropattern chips.

(B) Representative immunofluorescence staining of 80, 140, 225, and 500 μm regions, showing markers for each cell line, Pou5f1, Cdx2, and Foxa1/2, respectively (80 μm, $n = 62$ regions; 140 μm, $n = 35$ regions; 225 μm, $n = 25$ regions; 500 μm, $n = 4$ regions).

(C) Density plot showing average distribution of cells in normalized coordinate space for each marker and different sized regions.

(D) Distribution of total cells positive for each marker per region.

(E) Ratio of total cells positive for each marker per region. All scale bars indicate 40 μm.

investigate how induction of cell fate by CRISPRa changes migratory behavior of cells, we measured motion of cells by mean absolute displacement over time (Figure 3G). We observed a difference in displacement mainly for CRISPRa-induced sgGata6-mESCs over time when compared with no dox controls, suggesting an enhanced cellular motion upon cell-fate induction by CRISPRa. An increase in displacement appeared to co-occur with sgGata6-mESCs migrating to the edge at around 16–24 h of induction, while a decrease in displacement was observed at the end of the experiment, suggesting that sgGata6 cells arriving at the micropattern edge are less motile. Unlike sgCdx2-mESCs cells that form localized clusters, the increase in the angular movement of the sgGata6-mESCs demonstrates a coordinated behavior characterized by outward and rotational

Please cite this article in press as: Lodewijk et al., Self-organization of mouse embryonic stem cells into reproducible pre-gastrulation embryo models via CRISPRa programming, Cell Stem Cell (2025), https://doi.org/10.1016/j.stem.2025.02.015

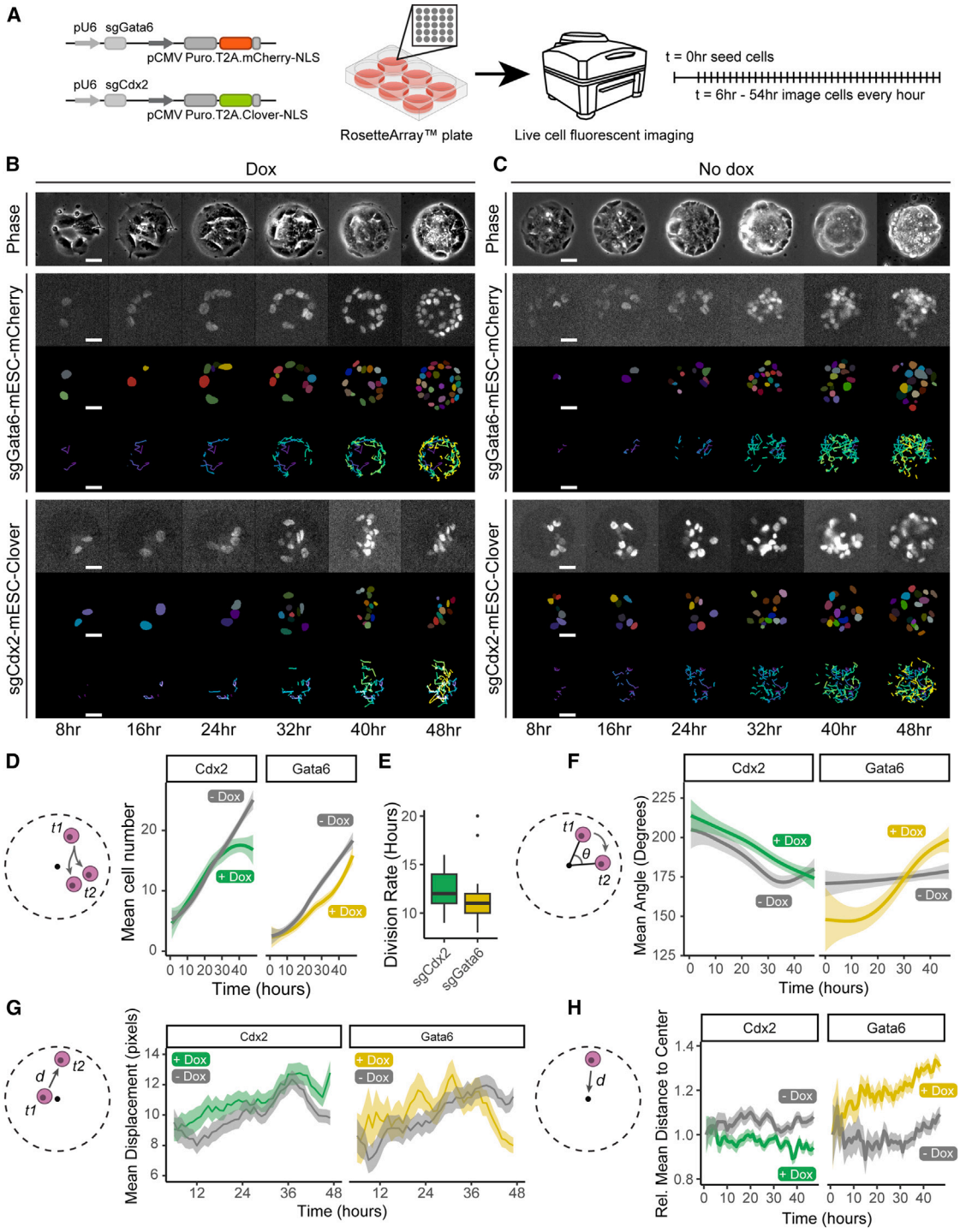

Figure 3. Live cell imaging and tracking in 2D micropatterns

(A) Overview of modified sgRNA constructs for tracking and imaging design.

(B and C) (B) Example timelapse images from a +dox (left) and (C) −dox (right) micropattern, showing phase contrast (top), sgGata6-mESCs (middle), and sgCdx2-mESCs (bottom). For sgGata6-mESC and sgCdx2-mESC panels, the top rows are fluorescent signals, the middle rows are segmented nuclei, and the bottom rows are cell tracking over time (tracks are colored to indicate time).

(D) Cell proliferation measured by the mean (±SEM) number of sgCdx2-mESCs and sgGata6-mESCs over time.

(E) Cell cycle duration in hours between divisions for sgCdx2 cells +dox (n = 35) and sgGata6 cells +dox (n = 37).

(legend continued on next page)

Please cite this article in press as: Lodewijk et al., Self-organization of mouse embryonic stem cells into reproducible pre-gastrulation embryo models via CRISPRa programming, Cell Stem Cell (2025), https://doi.org/10.1016/j.stem.2025.02.015

movements, resulting in the formation of boundary-like structures (Figure 3H). Over time, these cells increasingly align their motion to encircle other cells, forming a ring-like arrangement similar to natural XEN cells undergoing collective migration to encapsulate epiblast and trophoblast cells.[44,56] The single-cell live imaging shows that intrinsic fate induction in a few randomly positioned cells can generate orchestrated motion and growth, forming 2D patterns resembling peri-implantation embryonic patterning and highlighting the role of dynamic cellular movement in mammalian pattern formation.

Generation of 3D CPEMs

Based on our findings that CRISPRa-induced cells form 2D embryonic patterns, we reasoned that this approach can be used to form 3D embryo-like structures. To this end, we plated sgGata6-mESCs, sgCdx2-mESCs, and sgCtrl-mESCs in a 1:3:1 ratio in microwell plates (AggreWell 400). We performed immunostaining and confocal imaging 72 h after CRISPRa induction to visualize the spatial organization of 3D structures (Figure 4A). The results showed that CRISPRa-induced cells self-organize into embryo-like structures resembling embryos at 5–6 days post-fertilization (Figure 4B; Video S2A) and similar to other mouse embryo models.[5,28,29] We observed Foxa1/2+ cells (sgGata6-mESCs) forming an outer layer around radially patterned Pou5f1+ cells (sgCtrl-mESCs) and clusters of Cdx2+ cells (sgCdx2-mESCs). By segmenting 21,477 labels from single-cell nuclei across z-positions from 30 CPEMs and plotting the average density at each z-position, we confirmed self-organization of three CRISPRa-induced cell lines into embryo-like structures with asymmetric distribution of the three cell types along the z axis (Figure 4C) akin to proximal-distal axis in the egg cylinder stage of mouse embryonic development. By quantifying nuclear staining (DAPI) across the center z-position (Figure 4D), we observe cavity formation in 80% of structures (Figures 4E and 4F). CPEMs show consistent size of 100 μm in the z axis and 150 μm in x axis and y axis (longest axis) (Figure S4A). Structures show an approximately equal amount, 40%–50% each, of Foxa1/2+ cells and Pou5f1+ cells, and 10%–20% Cdx2+ cells (Figures 4G and 4H). Analyzing cellular positioning along the z axis revealed that Pou5f1+ and Cdx2+ cells resided in opposing sides of the structure (Figures 4I and 4J). Despite starting out with 3 times more sgCdx2-mESCs, these cells are the least prevalent in the 3D structures, suggesting that sgCdx2-mESCs undergo selection by slow growth, death, or delay in their development (Figures 4G and 4H).

The 1:3:1 (sgCtrl-:sgCdx2-:sgGata6-mESCs) ratio of starting cells was shown to be optimal in previously reported embryo models.[2,5,28,29] To investigate how cellular composition affects morphological features of CPEMs, we generated embryo models with different ratios of cell types and models composed of only one cell type. We observed that in the 1:1:3 condition (sgGata6-mESC overrepresented), CPEMs were slightly larger, whereas CPEMs from sgCtrl-only-mESCs or sgCdx2-only-mESCs appeared smaller (Figure S4A), resulting also in changes in cell ratios between conditions (Figure S4B). In the 1:1:3 ratio, we found that CPEMs formed larger cavities (Figure S4C). The opposite was true when changing the ratio to 3:1:1, where the sgCtrl-mESCs are overrepresented, and we found additional Pou5f1+ Epi-like cells ectopically growing, filling up cavities (Figure S4D). When using sgCtrl-mESCs alone (Figure S4F; Video S2B) or sgCdx2-mESCs alone (Figure S4G; Video S2C), no discernible embryonic patterns were observed. A small percentage of Foxa1/2+ cells were observed in these conditions, likely due to accelerated spontaneous differentiation in 3D aggregates; however, they did not form distinct spatial organizations. In the sgCdx2-mESC CPEMs, a subset of cells was Pou5f1/Cdx2 double-positive (Figure S4H), suggesting incomplete differentiation of some cells. The persistence of Pou5f1 expression in a subset of sgCdx2-mESCs highlights a limitation in fully differentiating into TSCs during the 3 days of doxycycline treatment (a revised protocol with enhanced TSC differentiation is described later). These findings underscore the importance of cellular composition in determining the size and spatial organization of embryo-like structures. Quantitative single-cell maps show that CPEMs closely resemble E5–E6 mouse embryos in cellular composition and morphology. Our findings also demonstrate that Gata6-expressing cells alone can induce cavity formation, highlighting their role in CPEM morphology.

Single-cell transcriptomics uncovers cell types and intercellular signaling of pre-gastrulation embryonic cells

To examine the differentiation of cells in CPEMs, we performed single-cell RNA sequencing (scRNA-seq). Unsupervised dimensionality reduction of single-cell transcriptomics of CPEMs resolved 6 clusters that were separated by expression of CRISPRa-induced target genes (Figure 5A). We identified three distinct populations marked by Nanog, Cdx2, and Gata6 expression, corresponding to the mix of three cell types to generate CPEMs (Figure 5A). We observed two clusters of Nanog-expressing cells, annotated as Epi1 and Epi2, with transcriptional resemblance to embryonic epiblast cells, as shown by the expression of Nanog, Pou5f1, Sox2, and Otx2 (Figure 5B). The two clusters likely reflect different stages of the cell cycle (Figure S5A). Gata6-expressing cells separated into two clusters, annotated as XEN1 and XEN2. XEN1 is enriched for embryonic visceral endoderm (emVE) markers Otx2, Cer1, and Lhx1, whereas XEN2 is enriched for extraembryonic visceral endoderm (exVE) markers, like Pdgfra and Sox17 (Figure 5B), resembling XEN development in natural embryos.[44] Similarly, two distinct populations of Cdx2-expressing cells were observed, annotated as TS1 and TS2 (Figure 5B). Cells in TS2 enriched for Id2, Pdgfa, and Tfap2c are related to canonical differentiation of TSCs, whereas the Cdx2+ cluster TS1 with higher Wnt5a expression showed lower levels of trophoblast markers, indicating a subpopulation of TSC formation upon Cdx2 induction,[27,57–60] or a cell population with delayed differentiation. A subset of CRISPRa-induced sgCdx2-mESCs maintained the expression of pluripotency

(F) Directionality of displacements measured by mean degree angles (±SEM) over time.
(G) Mean displacement (±SEM) of sgCdx2-mESCs and sgGata6-mESCs over time.
(H) Relative mean distance to center (±SEM) of sgCdx2-mESCs and sgGata6-mESCs over time. n = 11 micropattern regions per condition. Labels measured across all time points: +dox sgCdx2 n = 6,856, +dox sgGata6 n = 3,478, −dox sgCdx2 n = 7,482, −dox sgGata6 n = 4,918. All scale bars indicate 40 μm.

Please cite this article in press as: Lodewijk et al., Self-organization of mouse embryonic stem cells into reproducible pre-gastrulation embryo models via CRISPRa programming, Cell Stem Cell (2025), https://doi.org/10.1016/j.stem.2025.02.015

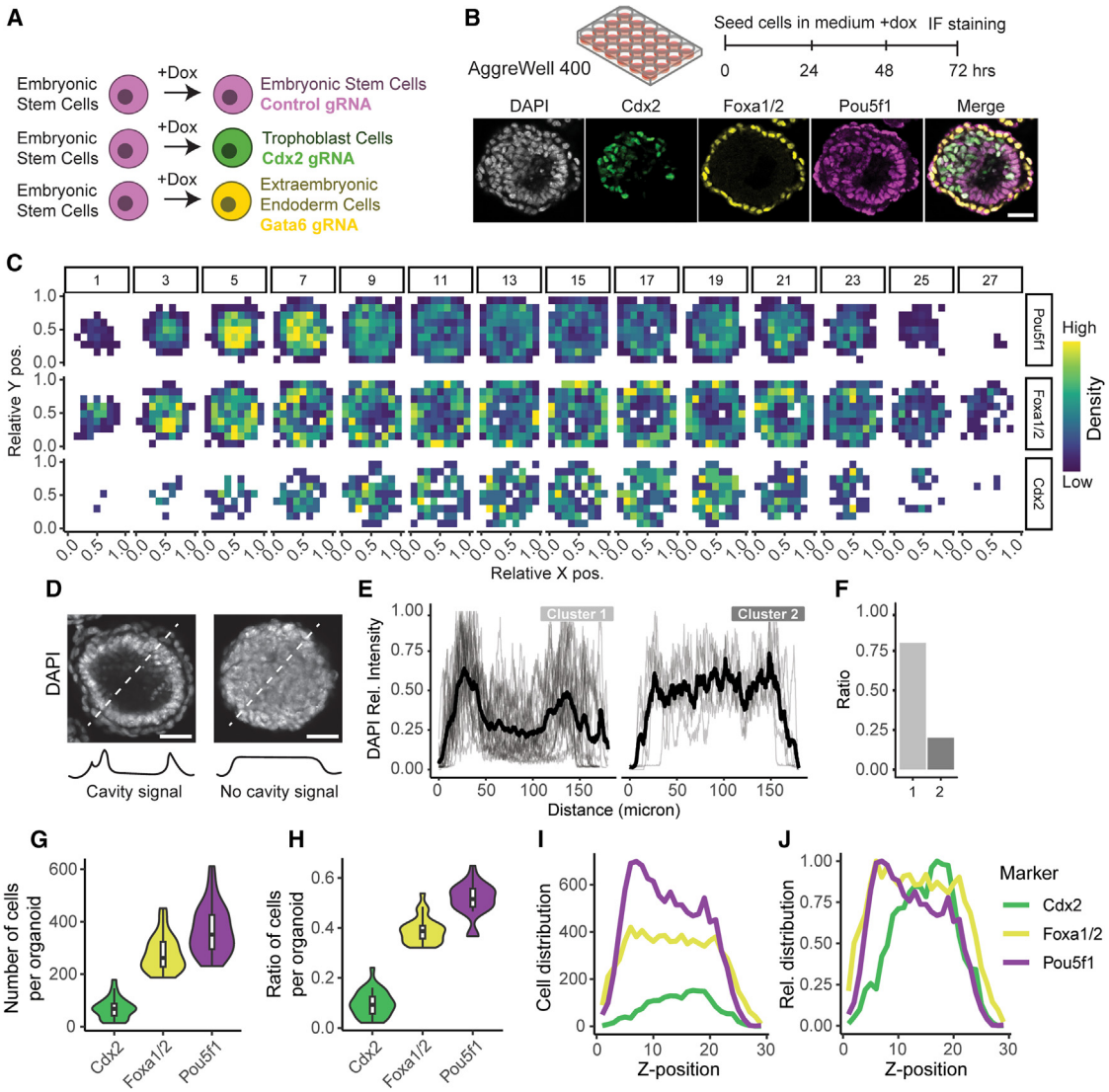

Figure 4. Generation and single-cell analysis of CPEMs

(A) Overview of cells used for differentiation.

(B) Differentiation protocol and representative confocal image of a CPEM, stained by Pou5f1, Cdx2, and Foxa1/2.

(C) Quantification of cell density for each marker across CPEMs using z stack confocal imaging (n = 30 CPEMs, n = 21,477 nuclei labels), left to right shows increasing depth with z stack steps (3.89 μm intervals, see z-position number above each plot), displaying every other step. Each plot shows the average cell density per staining, normalized in x-y-z coordinates.

(D) Cavity formation analysis by measuring DAPI staining in the center stack position of CPEMs, showing an example with (left) and without (right) cavity.

(E and F) (E) Quantification and clustering of cavity formation in two clusters, and (F) ratio of the clusters.

(G and H) (G) Number and (H) ratio of Cdx2, Foxa1/2, and Pou5f1 labeled cells identified in CPEMs.

(I) Mean number of Cdx2, Foxa1/2, and Pou5f1 labeled cells across imaged z-positions (n = 30 CPEMs).

(J) Relative distribution of Cdx2, Foxa1/2, and Pou5f1 labeled cells across imaged z-positions scaled to maximum within each group. n = 30 CPEMs measured. All scale bars indicate 40 μm.

factors such as Nanog and Pou5f1(Oct4), potentially due to delayed differentiation (Figure 5B).

To compare the transcriptional profiles of CPEM cell clusters to the natural embryo, we used canonical correlation analysis (CCA) to project cell types from CPEMs onto a reference dataset of published E5.25 mouse embryos.[61] This demonstrated that cells in CPEMs globally resemble those of natural embryos (Figures S5B–S5D). For benchmarking, we compared the transcriptome of 3-day CPEMs with a mouse embryo model formed by combining ESCs, TSCs, and XEN cells (ETX)[28] alongside the published E5.25 mouse embryo data. We observed a general agreement between expression of markers for different cell clusters between CPEM, ETX, and natural E5.25 mouse embryos (Figures 5B–5F). Both CRISPRa-induced XEN cells in CPEMs and mouse natural embryo XEN clusters exhibit separation into emVE

Please cite this article in press as: Lodewijk et al., Self-organization of mouse embryonic stem cells into reproducible pre-gastrulation embryo models via CRISPRa programming, Cell Stem Cell (2025), https://doi.org/10.1016/j.stem.2025.02.015

CellPress
OPEN ACCESS

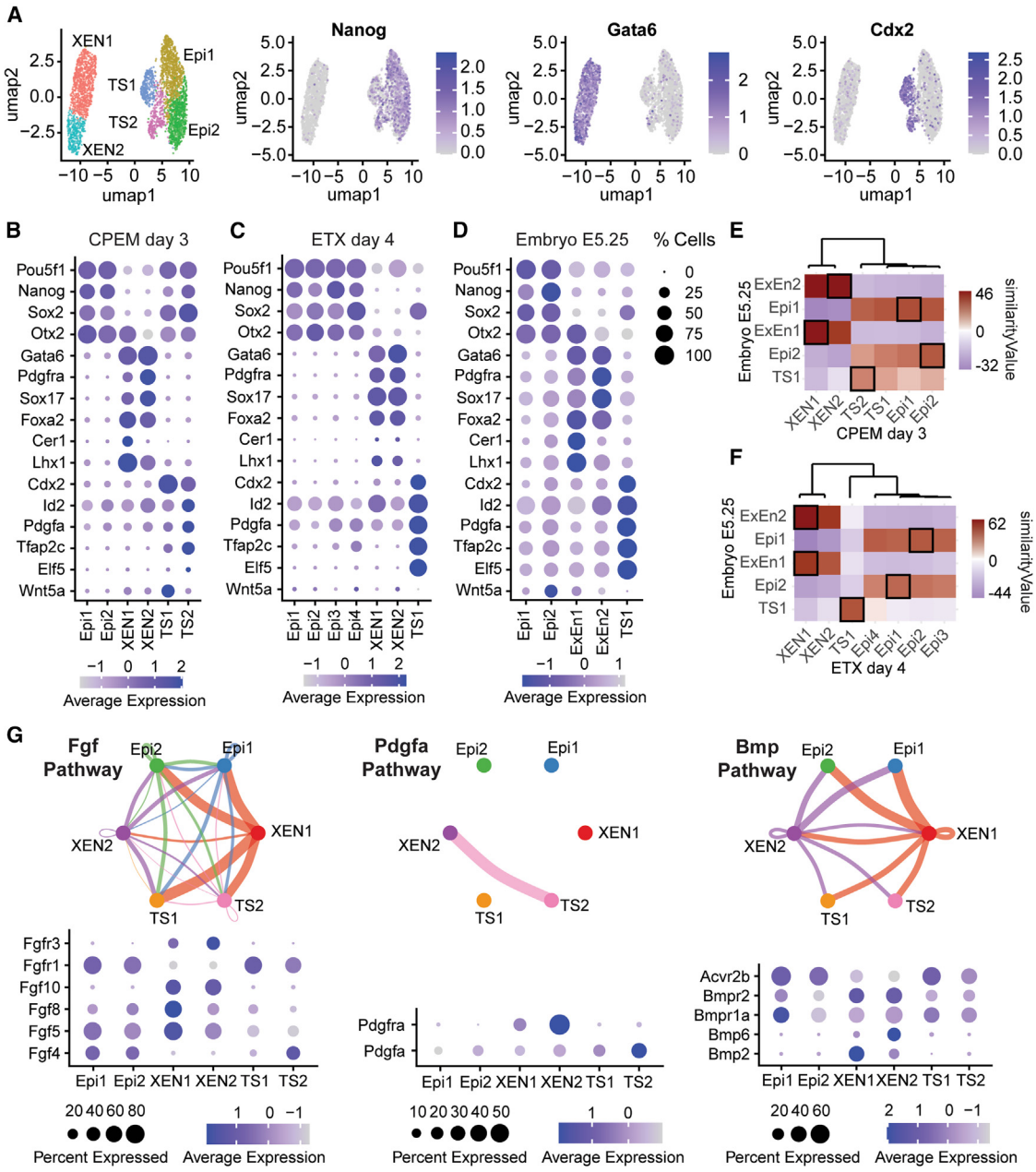

Figure 5. Comparative scRNA-seq analysis of 3D CPEMs and ligand-receptor interactions

(A) Uniform manifold approximation and projection (UMAP) and clustering analysis of scRNA-seq data of CPEMs, showing feature maps for Nanog, Gata6, and Cdx2.

(B) Dot plot showing a set of gene marker levels for Epi, TS, and XEN cells in CPEM scRNA-seq data.

(C) Markers levels in day 4 ETX scRNA-seq.

(D) Marker levels in E5.25 mouse embryo scRNA-seq. ExEn, extraembryonic endoderm of the natural embryo.

(E) Heatmap showing similarity scores from pairwise comparison between cell clusters from E5.25 mouse embryo and day 3 CPEM, and black outlines indicate the highest similarity pairs.

(F) Heatmap showing similarity scores from pairwise comparison between cell clusters from E5.25 mouse embryo and day 4 ETX.

(G) CellChat analysis showing ligand-receptor interactions between cell clusters of pathways known in early embryogenesis.

and exVE populations based on selected marker expression profiles. The specialization into emVE cells was less pronounced for the XEN cells of day 4 ETX embryo model generated by cDNA overexpression of Gata6 and Fgfr2 (Figures 5C and 5D). While TSCs in ETX embryo models and natural embryos are largely negative for the Epi markers Pou5f1 and Nanog, CRISPRa-induced TSCs in CPEMs exhibited persistent expression of these markers. The transcriptional similarity

Please cite this article in press as: Lodewijk et al., Self-organization of mouse embryonic stem cells into reproducible pre-gastrulation embryo models via CRISPRa programming, Cell Stem Cell (2025), https://doi.org/10.1016/j.stem.2025.02.015

between ETX model TSCs and those in natural embryos is likely due to the use of TSC lines derived directly from natural mouse embryos, rather than being induced from ESCs.

Next, we performed comparisons between single-cell transcriptomes using the ClusterFoldSimilarity package.[62] This revealed CPEM and mouse embryo XEN clusters match accordingly, showing that XEN cells in CPEMs cluster with emVE-like and exVE-like lineages (Figure 5E). Comparing ETX to the mouse embryo, both ETX XEN clusters score best with the same mouse XEN cluster, indicating XEN cells generated via cDNA overexpression of Gata6 cells have a slightly less pronounced separation into emVE and exVE lineages when compared with CRISPRa (Figure 5F). This indicates that CRISPRa-induced cells achieve a more refined separation of XEN lineages compared with cDNA-induced cells in the ETX model.

In the scRNA-seq data of CPEMs, sgCdx2-marked clusters showed transcriptional profiles similar to TSCs from natural embryos; however, CPEM TSC clusters had potential features of incomplete or delayed differentiation, for example, by retained Pou5f1 expression (Figures 5B–5F). Comparison of CRISPRa induction of Cdx2 with direct cDNA overexpression showed that CRISPRa achieves close expression level to mouse embryo-derived lines, whereas 3-day Cdx2 cDNA-expressing mESCs had lower Cdx2 expression[2] (Figure S5E).

Additionally, we examined the transcriptional profiles of CPEMs derived from single-cell types (Figures S5F–S5N). CPEMs from sgCtrl-mESCs showed no significant differentiation, with three Epi clusters linked to cell cycle phases and slightly altered pluripotency marker expression in the Epi2 cluster (Figures S5F and S5G). In sgGata6-mESC CPEMs, only XEN cells were identified. The XEN1 and XEN2 clusters showed overall similar features resembling emVE (enriched for Otx2, Foxa2, and Lhx1), and XEN3 resembled exVE (enriched for Sox17 and Pdgfra). XEN1 and XEN2 also exhibited cell cycle differences (Figures S5H and S5I). In sgCdx2-mESCs only aggregates, most cells were Cdx2-positive, while some retained epiblast markers, and two TS clusters showed marker expression similar to mixed-cell CPEMs (Figures S5J and S5K). While CPEMs grown in mixed or single-lineage cultures showed global transcriptional similarity (Figures 5B and S5L–S5N), subtle differences in cluster cell number and gene marker levels suggest cell-cell interactions influence the formation of cell subtypes.

We hypothesized that co-development of CRISPRa-induced cells can facilitate signaling crosstalk between cell types during formation into embryonic patterns.[8,14,63,64] To analyze potential signaling interactions between cells, we used CellChat[65] to analyze the expression of ligand-receptor pairs. We found predicted activity of pathways known to regulate early embryogenesis, such as the fibroblast growth factor (Fgf), platelet-derived growth factor (Pdgf), and bone morphogenetic protein (Bmp) pathway[49,66–71] (Figure 5G). We also detected paired expression of ligand-receptors in pathways that are less studied in early embryogenesis, such as Hedgehog, non-canonical Wnt signaling, and Plexin-Semaphorin pathways[72–75] (Figure S5O; Table S1). A subset of pathways identified originates from specific clusters of XEN cells and TSCs and targets other lineages, highlighting the presence of lineage-specific signaling centers that guide embryonic development. One example of a potential functional pairing is Semaphorin signaling, which was recently shown to instruct XEN migration.[76] Additionally, Pdgfa signaling from TS to XEN cells may promote their differentiation into exVE over emVE.[44,70] Supporting this, we observe a higher ratio of exVE in CPEMs grown from mixed cells (30% exVE-like) compared with sgGata6-induced cells only, which do not receive TSC signals (15% exVE-like) (Figure S5P). Thus, we captured multiple signaling pathways that link extraembryonic and embryonic cells, which may contribute to differentiation and spatial organization of cells in CPEMs.

Enhancing trophoblast differentiation and integration through extended CRISPRa induction and multiplexed activation of Cdx2 and Elf5

Our scRNA-seq and immunostaining analyses showed that trophoblast-like compartments of day 3 CPEMs contain a subset of sgCdx2 cells with residual expression of pluripotency factors, like Pou5f1(Oct4) (Figures 4B, 5A, and 5B). To address this, we extended the duration of CRISPRa induction and tested simultaneous activation of other trophoblast-fate determining factors. First, we used a 2-day dox pre-treatment of the sgCdx2-mESC before assembling the CPEMs (pre-induction) to test if longer Cdx2 activation, 5 days total in day 3 CPEMs, leads to more complete differentiation, as reported previously.[2] Second, we hypothesized that trophoblast differentiation can be accelerated by simultaneous activation of the Cdx2 and Elf5 promoters. The activation of Elf5 downstream of Cdx2, driven by demethylation of the Elf5 promoter, is a pivotal step in the development of TSCs.[2,57,77–79] In the sgCdx2:sgElf5 dual line, we also used the 2-day dox pre-treatment to compare with sgCdx2 CRISPRa alone (Figure 6A). We reconfirmed with no dox pre-treatment, Cdx2+ cells show remaining Pou5f1(Oct4) labeling (Figures 6B and 6C). When pre-treating with dox for 2 days, the remaining staining for Epi markers, Pou5f1 and Nanog, was lost (Figures 6B, 6C, S6A, and S6B), and cells were positive for Tfap2c and Gata3 (Figure S6C). We also observed higher ratios of Cdx2+ cells in CPEMs (Figure 6D) and an increase in CPEMs with more than 10% of total cells labeled as Cdx2+ (Figure S6D). Dual activation of Cdx2 and Elf5 without the 2-day dox pre-treatment did not have major effects on the number of TSCs (Figures 6B–6D and S6D). However, the 2-day dox pre-treatment with dual Cdx2 and Elf5 activation doubled the integration of Cdx2+ cells in CPEMs, compared with 2-day dox pre-treatment of Cdx2 activation only (Figure 6D). Under the 2-day pre-induced dual Cdx2/Elf5 condition, almost 75% of CPEMs had at least a 10% Cdx2+ cell contribution (Figure S6D) and showed clear opposite asymmetric profiles for Pou5f1 and Cdx2 (Figures S6E and S6F). We observed that in 70%–75% of CPEMs with at least 10% Cdx2 cell contribution, Cdx2+ cells are in a distinct domain resembling the structure in the mouse egg cylinder (Figures S6G and S6H). These data suggest there remains a time constraint in the differentiation of mESCs to TSCs when using Cdx2 activation or Cdx2/Elf5 dual activation. Importantly, simultaneous activation of multiple cell-fate determining factors with CRISPRa enhanced integration of mouse TSCs in CPEMs.

Formation of anterior signaling centers in CPEMs with enhanced TSCs

Next, we investigated whether CPEMs with enhanced trophoblast compartments establish anterior signaling centers,

Please cite this article in press as: Lodewijk et al., Self-organization of mouse embryonic stem cells into reproducible pre-gastrulation embryo models via CRISPRa programming, Cell Stem Cell (2025), https://doi.org/10.1016/j.stem.2025.02.015

CellPress
OPEN ACCESS

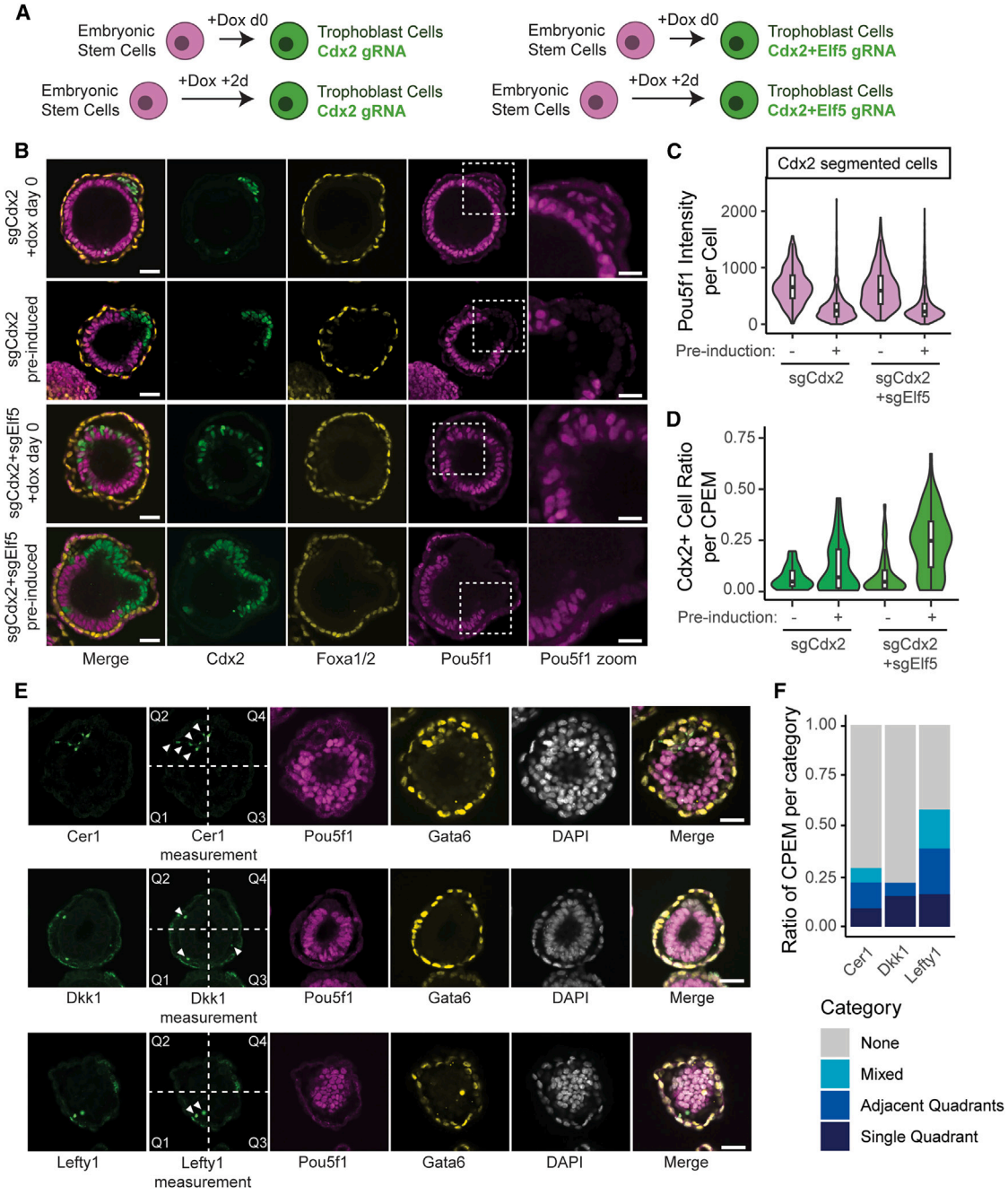

Figure 6. Improvements of CPEM TS compartment and characterization of AVE-like signaling

(A) Strategies to improve differentiation into TSCs by CRISPRa pre-induction and dual activation of Cdx2 and Elf5.

(B) Example staining of CPEMs grown with sgCdx2-mESCs, sgCdx2+sgElf5-mESCs, and with pre-induction.

(C) Quantification of Pou5f1 intensity per Cdx2-segmented cell across conditions. Number of cells analyzed per condition, sgCdx2: $n = 375$, sgCdx2 pre-induced: $n = 1,097$, sgCdx2 + sgElf5: $n = 529$, sgCdx2 + sgElf5 pre-induced: $n = 3,229$.

(D) Cdx2+ cell ratio per CPEM across conditions. Number of CPEMs analyzed per condition, sgCdx2: $n = 47$, sgCdx2 pre-induced: $n = 53$, sgCdx2 + sgElf5: $n = 53$, sgCdx2 + sgElf5 pre-induced: $n = 80$.

(E) Example staining of Cer1 (top), Dkk1 (middle), and Lefty1 (bottom) and their classification based on location within quarters of CPEMs.

(F) Quantification of Cer1, Dkk1, and Lefty1 by regionalized expression. CPEMs analyzed per staining, Cer1: $n = 55$, Dkk1: $n = 46$, Lefty1: $n = 31$. Scale bars indicate 40 μm, and zoom scale bars indicate 20 μm.

Please cite this article in press as: Lodewijk et al., Self-organization of mouse embryonic stem cells into reproducible pre-gastrulation embryo models via CRISPRa programming, Cell Stem Cell (2025), https://doi.org/10.1016/j.stem.2025.02.015

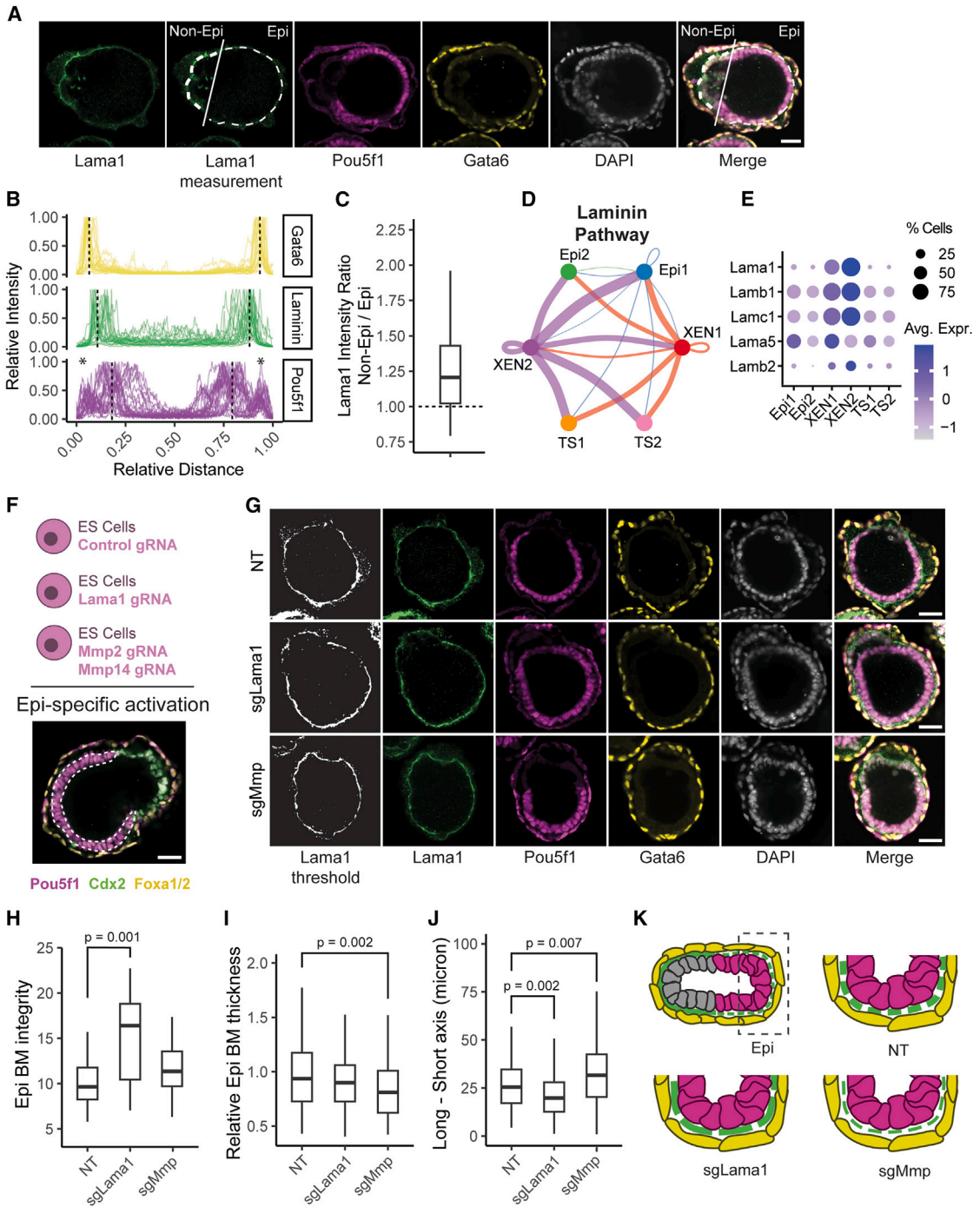

Figure 7. Modulation of BM in the Epi compartment of CPEMs using CRISPRa

(A) Example laminin staining in CPEMs, localization was measured across the image (full line), whereas laminin-specific measurements were done on the perimeter (dashed line).

(B) Staining of Gata6 (XEN), Lama1 (BM), and Pou5f1 (epiblast), showing Lama1 staining is separating XEN and Epi cells. Dashed lines indicate peak average signal per condition. Asterisks indicate non-specific labeling on the outside of CPEMs, $n = 19$.

(C) Relative Lama1 intensity of Epi and non-Epi (trophoblast) compartments, $n = 28$.

(D) CellChat output of laminin pathway in CPEM scRNA-seq data.

(E) Dot plot of laminin gene expression in CPEM scRNA-seq data.

(F) Schematic showing sgCtrl-mESC (epiblast, dashed line) replacement by CRISPRa mESCs with sgRNAs for Lama1 or Mmp2/Mmp14.

(G) Representative images of CPEM grown with sgCtrl- (NT), sgLama1-, or sgMmp-mESCs as Epi compartment, showing thresholded Lama1 staining for comparison.

(legend continued on next page)

Please cite this article in press as: Lodewijk et al., Self-organization of mouse embryonic stem cells into reproducible pre-gastrulation embryo models via CRISPRa programming, Cell Stem Cell (2025), https://doi.org/10.1016/j.stem.2025.02.015

analogous to those formed by the AVE in natural embryos. Local expression of Lefty1, Cer1, and Dkk1 starting around embryonic days 5 instructs symmetry breaking through inhibition of Wnt and Nodal signaling in a subset of epiblast cells and initiates gastrulation.[76,80] We found expression of Cer1 in a subset of XEN cells (Figure S6I) and also identified Gata6, Foxa1/2, Sox17, Lhx1, and Pdgfra in sgGata6-induced XEN cells (Figures S6J–S6L). Immunostaining for Lefty1, Dkk1, and Cer1 (Figure 6E) shows that about 50% of CPEMs are Lefty1+ and around 25% are Cer1+ or Dkk1+. These stainings suggest some degree of localized signaling, resembling aspects of pre-gastrulation patterning observed in natural embryos (Figures 6E and 6F). Additionally, Pdgfra expression was regionalized, similar to XEN of the mouse egg cylinder (Figures S6M and S6N).[70] However, not all CPEMs showed signs of anterior axis formation, likely due to variability in developmental timing or incomplete specification of AVE-like signaling centers. These findings highlight the potential of CPEMs to investigate formation of AVE signaling centers and early anterior axis formation.

Basement membrane formation in CPEMs and its remodeling via CRISPRa of laminin and Mmp

To further characterize the structural properties of CPEMs, we investigated whether CPEMs form the basement membrane (BM), a crucial component for embryonic structural integrity, boundary formation, and signaling in natural embryos.[81–85] To test this, we performed immunostaining to visualize laminin alpha 1 (Lama1), a key protein for BM formation. Lama1 staining was observed in nearly all CPEMs, surrounding both the epiblast and trophoblast compartments (Figures 7A and 7B). Comparing the epiblast side with the non-epiblast side of CPEMs showed that laminin level is distributed asymmetrically with a slightly lower level in the epiblast side (Figure 7C). In addition, staining for E-cadherin (Cdh1) further revealed that epiblast cells in CPEMs form clear adhesion bonds, enriched at interfaces within the structure, indicating successful boundary establishment similar to what has been reported in natural embryos[86,87] (Figure S7A).

The XEN and epiblast cells play a pivotal role in BM remodeling by producing matrix components like laminin and regulating its breakdown through the expression of Mmp to enable the elongated growth of the embryo cylinder. The Mmp2 and Mmp14 proteins are examples involved in this process.[85] In CPEM scRNA-seq data, we identify XEN clusters as major producers of laminins, including Lama1, Lamb1, and Lamc1 (Figures 7D and 7E). We hypothesized that altering the location of laminin production and degradation by ectopically activating laminin and Mmps in the epiblast compartment could impact BM remodeling and CPEM morphology.

To test this hypothesis, we used CRISPRa for lineage-specific activation of regulatory regions of Lama1 and Mmp2/Mmp14 within the epiblast compartment (Figure 7F). The Lama1 gene, a large 120 kb locus with 65 exons and multiple isoforms and coding for a protein of over 3,000 amino acids with repetitive domains, poses unique challenges for direct cDNA expression. CRISPRa efficiently induced Lama1 expression in mESCs cells through sgRNA targeting its gene promoter (Figures S7B and S7C). Similarly, we were able to activate Mmp2 and Mmp14 in mESCs (Figures S7D and S7E). Integrating these new mESCs as epiblast cells in CPEMs (Figure 7G), we found that with sgLama1-mESCs, the BM in CPEMs showed higher integrity as determined by decreased laminin gaps compared with CPEMs formed with sgCtrl-mESCs instead (Figure 7H). In a parallel experiment, we added equal amounts of sgMmp2-mESCs and sgMmp14-mESCs (labeled sgMmp). Overactivation of Mmp2/Mmp14 led to a decreased thickness of the BM (Figure 7I). In both cases, the non-epi compartment was not affected (Figures S7F and S7G), suggesting that the Epi-specific CRISPRa of Lama1 and Mmp2/Mmp14 is lineage-specific and acts locally. We observed reciprocal effects in general CPEM shape, where sgLama1 CPEMs were more rounded, and sgMmp CPEMs were slightly more elongated (Figure 7J). Our CRISPRa perturbation highlights the intricate balance of structural components of the BM to determine morphology of embryo models (Figure 7K). These results showcase the potential of CRISPR tools for precise epigenome activation in a lineage-specific manner in CPEMs, while underscoring its power for mechanistic studies.

DISCUSSION

As new frontiers are emerging in studying mammalian embryogenesis using SEMs, there is a need to complement and improve existing approaches to generate embryo models in a facile and controlled manner with enhanced reproducibility in spatial patterns and cellular compositions.[88,89] In this study we demonstrate that CRISPRa of two endogenous regulatory elements in ESCs is sufficient to self-organize embryonic patterns, presenting a simple CRISPRa-based approach to induce cell fates and form programmable embryo models. We show that co-culturing mESC lines expressing sgRNAs targeting Gata6, Cdx2, or non-targeting controls in a simple medium without external cues leads to spatial organization resembling pre-gastrulation mouse embryo. In our model, XEN cells (sgGata6-mESCs) surround TSC-like cells (sgCdx2-mESCs) and epiblast cells (sgCtrl-mESCs), with clear cavity formation in 3D models. Notably, sgGata6-induced XEN cells appear important for patterning, as their absence disrupts CPEM organization, and these cells alone can form cavitated structures in our model.

Timelapse fluorescent microscopy of 2D patterns revealed cell migration, leading to self-organized spatial patterns. Proliferating XEN cells formed a ring around the structure, while TS-like cells clustered internally, distinct from Epi-like cells. The increased angular movement of sgGata6-mESCs suggests that

(H) Measurement of BM integrity in CPEMs by average number of gaps in Lama1 staining along the Epi compartment. NT: $n = 26$, sgLama1: $n = 15$, sgMmp: $n = 17$ CPEMs.
(I) Measurement of relative BM thickness in CPEMs. NT: $n = 95$, sgLama1: $n = 71$, sgMmp: $n = 69$ CPEMs.
(J) Shape analysis of long and short axis in CPEMs. NT: $n = 108$, sgLama1: $n = 79$, sgMmp: $n = 84$ CPEMs.
(K) Schematic representation of sgLama1 and sgMmp activation in the Epi compartment of CPEMs. p values were calculated using Student's t test. All scale bars indicate 40 μm.

Please cite this article in press as: Lodewijk et al., Self-organization of mouse embryonic stem cells into reproducible pre-gastrulation embryo models via CRISPRa programming, Cell Stem Cell (2025), https://doi.org/10.1016/j.stem.2025.02.015

CRISPRa-induced XEN-like cells exhibit coordinated rotational motion, forming a boundary around epiblast and TSC-like cells, similar to XEN cells in natural embryos. Notably, XEN-like cells reproducibly organize only in smaller growth areas (80 or 140 μm) but not in larger ones (225 or 500 μm). Such coherent angular motion has been observed in other developmental contexts, like chicken embryo gastrulation[90] and development of mammary glands' acini structures,[91] underscoring their importance in morphogenesis during development. Although cellular motion might intuitively seem disruptive to pattern formation, our findings suggest that coordinated motion contributes to spatial organization during pattern formation in engineered systems and likely in natural embryos. Supporting this model, recent studies have shown that the sorting of epiblast and primitive endoderm cells within the inner cell mass relies on Rac1-dependent collective migration of cells that is likely guided by laminin deposition.[56] Additional mechanisms, like fluctuations in cellular surface tension and preferential cell-cell adhesion, also play roles in establishing embryonic patterning and robust boundary formation.[26,92] Compared with previous studies that investigate gastrulation using mouse and human ESCs in micropattern cultures, we also find radial organization of differentiated cells, in particular sgGata6-mESC-derived XEN-like cells. In the mouse gastrulation micropattern model, typically a mix of XEN and trophoblast is found at the edges[48]; however, in our model we have a ring-like structure formed only by XEN-like cells at the edge. This is likely due to the earlier developmental stage of our model, of early implantation, compared with the previous studies that represent mid-to-late stage gastrulation, suggesting the late-gastrulation stage cells, such as the primitive streak, likely have not formed yet in our model. The micropattern model in this study behaves like a 2D projection of the 3D CPEM model, aligning with early implantation and pre-gastrulation stages in structure and RNA profile. Additionally, the spatial separation of XEN and trophoblasts in natural embryos suggests limitations of late-stage 2D mouse gastrulation models in replicating embryonic spatial organization. Future micropattern studies could explore shapes like rectangles, enabling additional symmetry breaking and lineage separation, as shown in a recent gastrulation model[93] and neural tube formation.[94] This indicates that in the right environment, coordinated motion, growth, and intercellular signaling can induce self-organizing embryo-like structures without adding morphogens.

CPEMs display molecular similarities with recently published ETX embryo models that have grown for 3–4 days in organization and cell number.[5,29] Specifically, day 4 ETX models were previously shown to have about 500 Epi, 150 TS, and 350 XEN per structure, where we find our initial day 3 CPEMs contain about 350 Epi, 80 TS, and 280 XEN cells each. We also find the scRNA-seq data from our CPEMs can be mapped to cell types found in the E5.25 mouse embryo and find that sgGata6-mESC-derived XEN-like cells produce emVE-like and exVE-like cells and observe regional specialization into distal/anterior VE cells. However, trophoblast-like cells appeared immature in the original protocol. The relatively lower number of TSCs in our original model was significantly improved by pre-inducing the sgCdx2-mESCs for 2 days and via CRISPRa multiplexing to introduce a second sgRNA for dual activation of Cdx2 and Elf5 in the same mESCs.

CRISPR-based systems enhance existing methods by enabling physiological expression, multiplexed inputs, and rapid perturbations while overcoming epigenetic barriers to differentiation as hypothesized by Oldak et al.[16] For example, proper trophoblast differentiation in natural embryos and Cdx2-cDNA-induced TSCs requires Elf5 activation,[57,77–79] which we achieved in this study using CRISPRa targeting of Elf5. CRISPRa allows natural mRNA processing, ensuring cell-context specificity. Additionally, CRISPR tools expand (epi-)genetic circuits for cell specification, as shown by dual Cdx2/Elf5 activation. Their ability to target regulatory elements enables precise cell induction and lineage-specific perturbations in embryo models, as exemplified by modulation of Lama1 in our experiments. Integrating CRISPR into embryonic cells will facilitate large-scale screening of key fate determinants, enhancers, and signaling factors in spatial patterning.

Limitations of the study

We acknowledge limitations in this study, including background Cdx2 expression in sgCdx2-mESCs without doxycycline induction, which could be minimized through additional selection for low-background lines. Long-term CRISPR activity may be hindered by transgene silencing or loss of promoter activity in differentiated cells, which can be monitored with periodic efficiency testing. While we examined CPEM development for 3 days, extending culture duration could be explored in the future to test the development potential of CPEMs into gastrulation stages, assessing the potential for more pronounced and functional AVE-like activity. In 2D micropattern models, static growth areas limit long-term culture, as high cell densities after 3 days impede further growth and survival. Targeting multiple cell-type-specific regulatory elements could enhance differentiation fidelity and sub-lineage specification in embryo models or enable longer development under simple culture conditions. The CRISPR-Cas ortholog systems like Cas12a, which facilitate multiplexing,[95,96] could be used to better control cell subpopulations and potentially introduce missing cell types like trophoblast giant cells. Temporal control can be improved using protein degrons and combining CRISPRa and inhibition systems to create controllable gene circuits.

RESOURCE AVAILABILITY

Lead contact

Further information and requests for resources and reagents should be directed to and will be fulfilled by the lead contact, Dr. Ali Shariati (alish@ucsc.edu).

Materials availability

All unique/stable materials generated in this study are available from the lead contact upon reasonable request with a completed materials transfer agreement.

Data and code availability

- scRNA-seq data have been deposited at GEO as GEO: GSE256138 and are publicly available as of the date of publication.
- This paper analyzes existing, publicly available data, accessible at GEO: GSE206132 (ETX model scRNA-seq), GEO: GSE109071 (E5.25 embryo scRNA-seq), GEO: GSE208681 (Cdx2 cDNA-expressing mESC RNA-seq), ENA: PRJNA577068 (mouse blastocyst RNA-seq), and NGDC GSA: CRA000297 (mouse blastocyst DNAseI hypersensitivity).

- All original code has been deposited at Zenodo and is publicly available at https://doi.org/10.5281/zenodo.14511168 as of the date of publication.
- Any additional information required to reanalyze the data reported in this paper is available from the lead contact upon request.

ACKNOWLEDGMENTS

We would like to thank Dr. Camilla Forsberg, Dr. Russ Corbett-Detig, Dr. Seth Rubin, and Dr. Euiseok Kim for providing feedback on our manuscript. We also would like to thank the members of the Shariati lab for their feedback on the manuscript. We are also thankful to the IBSC and Genomics Institute leadership for their generous support in providing facilities and computational resources to complete this study. This work was supported by the NIH/NIGMS through a Pathway to Independence award K99GM126027/R00GM126027 and Maximizing Investigator Award (R35GM147395), a start-up package from the University of California, Santa Cruz (S.A.S.). G.A.L. is supported by a Dutch Research Council (NWO) Rubicon fellowship (019202en029). B.R.T. is supported by the National Institutes of Health (NIH) under award number K12GM139185 and the Institute for the Biology of Stem Cells (IBSC) at UC, Santa Cruz. G.K. and R.A. are supported by an NIH/NIEHS FastTrack STTR Award (R42ES033912). L.S.Q. is supported by an NSF CAREER award (#2046650) and an NIH NHGRI grant (#R21HG013133). L.S.Q. is a Chan Zuckerberg Biohub investigator. The content is solely the responsibility of the authors and does not necessarily represent the official views of the NIH or the IBSC. Technical support was provided from Benjamin Abrams, UCSC Life Sciences Microscopy Center, NIH S10 grant 1S10OD23528-01, RRID: SCR_021135.

AUTHOR CONTRIBUTIONS

S.A.S., G.A.L., and S.K. conceptualized the project, performed experiments, and analyzed the majority of the results. S.A.S. and G.A.L. wrote the manuscript and prepared the figures. C.J.H. performed immunostaining and analyzed confocal images of the 3D embryo models. A.Z. and S.L. contributed to the analysis of live imaging 2D micropattern experiments. L.N. helped with the cloning of sgRNAs for Lama1 and Mmp2/Mmp14 and TSC validation. L.S.Q. provided feedback on the manuscript and CRISPR resources. G.K. and R.A. fabricated the micropattern dishes used for live imaging experiments. B.R.T. set up initial experiments using 2D micropattern culture and reviewed the manuscript.

DECLARATION OF INTERESTS

G.K. and R.A. are co-founders of Neurosetta, which is focused on commercializing the RosetteArray platform. L.S.Q. is founder of Epicrispr Biotechnologies and scientific advisor of the Laboratory of Genomic Research and Kytopen Corp.

STAR★METHODS

Detailed methods are provided in the online version of this paper and include the following:

SUPPLEMENTAL INFORMATION

Supplemental information can be found online at https://doi.org/10.1016/j.stem.2025.02.015.

Received: March 5, 2024
Revised: December 17, 2024
Accepted: February 26, 2025
Published: March 20, 2025

REFERENCES

1. Rivron, N.C., Frias-Aldeguer, J., Vrij, E.J., Boisset, J.-C., Korving, J., Vivié, J., Truckenmüller, R.K., van Oudenaarden, A., van Blitterswijk, C.A., and Geijsen, N. (2018). Blastocyst-like structures generated solely from stem cells. Nature *557*, 106–111. https://doi.org/10.1038/s41586-018-0051-0.
2. Tarazi, S., Aguilera-Castrejon, A., Joubran, C., Ghanem, N., Ashouokhi, S., Roncato, F., Wildschutz, E., Haddad, M., Oldak, B., Gomez-Cesar, E., et al. (2022). Post-gastrulation synthetic embryos generated ex utero from mouse naive ESCs. Cell *185*, 3290–3306.e25. https://doi.org/10.1016/j.cell.2022.07.028.
3. Amadei, G., Handford, C.E., Qiu, C., De Jonghe, J., Greenfeld, H., Tran, M., Martin, B.K., Chen, D.-Y., Aguilera-Castrejon, A., Hanna, J.H., et al. (2022). Embryo model completes gastrulation to neurulation and organogenesis. Nature *610*, 143–153. https://doi.org/10.1038/s41586-022-05246-3.
4. Sozen, B., Cox, A.L., De Jonghe, J., Bao, M., Hollfelder, F., Glover, D.M., and Zernicka-Goetz, M. (2019). Self-organization of mouse stem cells into an extended potential blastoid. Dev. Cell *51*, 698–712.e8. https://doi.org/10.1016/j.devcel.2019.11.014.
5. Sozen, B., Amadei, G., Cox, A., Wang, R., Na, E., Czukiewska, S., Chappell, L., Voet, T., Michel, G., Jing, N., et al. (2018). Self-assembly of embryonic and two extra-embryonic stem cell types into gastrulating embryo-like structures. Nat. Cell Biol. *20*, 979–989. https://doi.org/10.1038/s41556-018-0147-7.
6. Lau, K.Y.C., Rubinstein, H., Gantner, C.W., Hadas, R., Amadei, G., Stelzer, Y., and Zernicka-Goetz, M. (2022). Mouse embryo model derived exclusively from embryonic stem cells undergoes neurulation and heart development. Cell Stem Cell *29*, 1445–1458.e8. https://doi.org/10.1016/j.stem.2022.08.013.
7. Shahbazi, M.N., Siggia, E.D., and Zernicka-Goetz, M. (2019). Self-organization of stem cells into embryos: A window on early mammalian development. Science *364*, 948–951. https://doi.org/10.1126/science.aax0164.
8. Wei, Y., Zhang, E., Yu, L., Ci, B., Sakurai, M., Guo, L., Zhang, X., Lin, S., Takii, S., Liu, L., et al. (2023). Dissecting embryonic and extraembryonic lineage crosstalk with stem cell co-culture. Cell *186*, 5859–5875.e24. https://doi.org/10.1016/j.cell.2023.11.008.
9. Beccari, L., Moris, N., Girgin, M., Turner, D.A., Baillie-Johnson, P., Cossy, A.-C., Lutolf, M.P., Duboule, D., and Arias, A.M. (2018). Multi-axial

self-organization properties of mouse embryonic stem cells into gastruloids. Nature *562*, 272–276. https://doi.org/10.1038/s41586-018-0578-0.

10. ten Berge, D., Koole, W., Fuerer, C., Fish, M., Eroglu, E., and Nusse, R. (2008). Wnt signaling mediates self-organization and axis formation in embryoid bodies. Cell Stem Cell *3*, 508–518. https://doi.org/10.1016/j.stem.2008.09.013.
11. van den Brink, S.C., Baillie-Johnson, P., Balayo, T., Hadjantonakis, A.-K., Nowotschin, S., Turner, D.A., and Martinez Arias, A. (2014). Symmetry breaking, germ layer specification and axial organisation in aggregates of mouse embryonic stem cells. Development *141*, 4231–4242. https://doi.org/10.1242/dev.113001.
12. Liu, X., Tan, J.P., Schröder, J., Aberkane, A., Ouyang, J.F., Mohenska, M., Lim, S.M., Sun, Y.B.Y., Chen, J., Sun, G., et al. (2021). Modelling human blastocysts by reprogramming fibroblasts into iBlastoids. Nature *591*, 627–632. https://doi.org/10.1038/s41586-021-03372-y.
13. Kagawa, H., Javali, A., Khoei, H.H., Sommer, T.M., Sestini, G., Novatchkova, M., Scholte op Reimer, Y., Castel, G., Bruneau, A., Maenhoudt, N., et al. (2022). Human blastoids model blastocyst development and implantation. Nature *601*, 600–605.
14. Hislop, J., Song, Q., Keshavarz F, K., Alavi, A., Schoenberger, R., LeGraw, R., Velazquez, J.J., Mokhtari, T., Taheri, M.N., Rytel, M., et al. (2024). Modelling post-implantation human development to yolk sac blood emergence. Nature *626*, 367–376. https://doi.org/10.1038/s41586-023-06914-8.
15. Warmflash, A., Sorre, B., Etoc, F., Siggia, E.D., and Brivanlou, A.H. (2014). A method to recapitulate early embryonic spatial patterning in human embryonic stem cells. Nat. Methods *11*, 847–854. https://doi.org/10.1038/nmeth.3016.
16. Oldak, B., Wildschutz, E., Bondarenko, V., Comar, M.-Y., Zhao, C., Aguilera-Castrejon, A., Tarazi, S., Viukov, S., Pham, T.X.A., Ashouokhi, S., et al. (2023). Complete human day 14 post-implantation embryo models from naïve ES cells. Nature *622*, 562–573. https://doi.org/10.1038/s41586-023-06604-5.
17. Yanagida, A., Spindlow, D., Nichols, J., Dattani, A., Smith, A., and Guo, G. (2021). Naive stem cell blastocyst model captures human embryo lineage segregation. Cell Stem Cell *28*, 1016–1022.e4. https://doi.org/10.1016/j.stem.2021.04.031.
18. Yu, L., Wei, Y., Duan, J., Schmitz, D.A., Sakurai, M., Wang, L., Wang, K., Zhao, S., Hon, G.C., and Wu, J. (2021). Blastocyst-like structures generated from human pluripotent stem cells. Nature *591*, 620–626. https://doi.org/10.1038/s41586-021-03356-y.
19. Sozen, B., Jorgensen, V., Weatherbee, B.A.T., Chen, S., Zhu, M., and Zernicka-Goetz, M. (2021). Reconstructing aspects of human embryogenesis with pluripotent stem cells. Nat. Commun. *12*, 5550. https://doi.org/10.1038/s41467-021-25853-4.
20. Simunovic, M., Metzger, J.J., Etoc, F., Yoney, A., Ruzo, A., Martyn, I., Croft, G., You, D.S., Brivanlou, A.H., and Siggia, E.D. (2019). A 3D model of a human epiblast reveals BMP4-driven symmetry breaking. Nat. Cell Biol. *21*, 900–910. https://doi.org/10.1038/s41556-019-0349-7.
21. Zheng, Y., Xue, X., Shao, Y., Wang, S., Esfahani, S.N., Li, Z., Muncie, J.M., Lakins, J.N., Weaver, V.M., Gumucio, D.L., et al. (2019). Controlled modelling of human epiblast and amnion development using stem cells. Nature *573*, 421–425. https://doi.org/10.1038/s41586-019-1535-2.
22. Moris, N., Anlas, K., van den Brink, S.C., Alemany, A., Schröder, J., Ghimire, S., Balayo, T., van Oudenaarden, A., and Martinez Arias, A. (2020). An in vitro model of early anteroposterior organization during human development. Nature *582*, 410–415. https://doi.org/10.1038/s41586-020-2383-9.
23. Simunovic, M., Siggia, E.D., and Brivanlou, A.H. (2022). In vitro attachment and symmetry breaking of a human embryo model assembled from primed embryonic stem cells. Cell Stem Cell *29*, 962–972.e4. https://doi.org/10.1016/j.stem.2022.05.001.
24. Yu, L., Logsdon, D., Pinzon-Arteaga, C.A., Duan, J., Ezashi, T., Wei, Y., Ribeiro Orsi, A.E., Oura, S., Liu, L., Wang, L., et al. (2023). Large-scale production of human blastoids amenable to modeling blastocyst development and maternal-fetal cross talk. Cell Stem Cell *30*, 1246–1261.e9. https://doi.org/10.1016/j.stem.2023.08.002.
25. Veenvliet, J.V., Bolondi, A., Kretzmer, H., Haut, L., Scholze-Wittler, M., Schifferl, D., Koch, F., Guignard, L., Kumar, A.S., Pustet, M., et al. (2020). Mouse embryonic stem cells self-organize into trunk-like structures with neural tube and somites. Science *370*, eaba4937. https://doi.org/10.1126/science.aba4937.
26. Bao, M., Cornwall-Scoones, J., Sanchez-Vasquez, E., Cox, A.L., Chen, D.-Y., De Jonghe, J., Shadkhoo, S., Hollfelder, F., Thomson, M., Glover, D.M., et al. (2022). Stem cell-derived synthetic embryos self-assemble by exploiting cadherin codes and cortical tension. Nat. Cell Biol. *24*, 1341–1349. https://doi.org/10.1038/s41556-022-00984-y.
27. Seong, J., Frias-Aldeguer, J., Holzmann, V., Kagawa, H., Sestini, G., Heidari Khoei, H., Scholte op Reimer, Y., Kip, M., Pradhan, S.J., Verwegen, L., et al. (2022). Epiblast inducers capture mouse trophectoderm stem cells in vitro and pattern blastoids for implantation in utero. Cell Stem Cell *29*, 1102–1118.e8. https://doi.org/10.1016/j.stem.2022.06.002.
28. Dupont, C., Schäffers, O.J.M., Tan, B.F., Merzouk, S., Bindels, E.M., Zwijsen, A., Huylebroeck, D., and Gribnau, J. (2023). Efficient generation of ETX embryoids that recapitulate the entire window of murine egg cylinder development. Sci. Adv. *9*, eadd2913. https://doi.org/10.1126/sciadv.add2913.
29. Amadei, G., Lau, K.Y.C., De Jonghe, J., Gantner, C.W., Sozen, B., Chan, C., Zhu, M., Kyprianou, C., Hollfelder, F., and Zernicka-Goetz, M. (2021). Inducible Stem-Cell-Derived Embryos Capture Mouse Morphogenetic Events In Vitro. Dev. Cell *56*, 366–382.e9. https://doi.org/10.1016/j.devcel.2020.12.004.
30. Pedroza, M., Gassaloglu, S.I., Dias, N., Zhong, L., Hou, T.J., Kretzmer, H., Smith, Z.D., and Sozen, B. (2023). Self-patterning of human stem cells into post-implantation lineages. Nature *622*, 574–583. https://doi.org/10.1038/s41586-023-06354-4.
31. Shahbazi, M.N., and Zernicka-Goetz, M. (2018). Deconstructing and reconstructing the mouse and human early embryo. Nat. Cell Biol. *20*, 878–887. https://doi.org/10.1038/s41556-018-0144-x.
32. Langkabel, J., Horne, A., Bonaguro, L., Holsten, L., Hesse, T., Knaus, A., Riedel, Y., Becker, M., Händler, K., Elmzzahi, T., et al. (2021). Induction of Rosette-to-Lumen stage embryoids using reprogramming paradigms in ESCs. Nat. Commun. *12*, 7322. https://doi.org/10.1038/s41467-021-27586-w.
33. Weatherbee, B.A.T., Gantner, C.W., Iwamoto-Stohl, L.K., Daza, R.M., Hamazaki, N., Shendure, J., and Zernicka-Goetz, M. (2023). Pluripotent stem cell-derived model of the post-implantation human embryo. Nature *622*, 584–593. https://doi.org/10.1038/s41586-023-06368-y.
34. Lambourne, L., Mattioli, K., Santoso, C., Sheynkman, G., Inukai, S., Kaundal, B., Berenson, A., Spirohn-Fitzgerald, K., Bhattacharjee, A., Rothman, E., et al. (2024). Widespread variation in molecular interactions and regulatory properties among transcription factor isoforms. Preprint at bioRxiv. https://doi.org/10.1101/2024.03.12.584681.
35. Liu, P., Chen, M., Liu, Y., Qi, L.S., and Ding, S. (2018). CRISPR-based chromatin remodeling of the endogenous Oct4 or Sox2 locus enables reprogramming to pluripotency. Cell Stem Cell *22*, 252–261.e4. https://doi.org/10.1016/j.stem.2017.12.001.
36. Liu, Y., Yu, C., Daley, T.P., Wang, F., Cao, W.S., Bhate, S., Lin, X., Still, C., 2nd, Liu, H., Zhao, D., et al. (2018). CRISPR activation screens systematically identify factors that drive neuronal fate and reprogramming. Cell Stem Cell *23*, 758–771.e8. https://doi.org/10.1016/j.stem.2018.09.003.
37. Pulecio, J., Verma, N., Mejía-Ramírez, E., Huangfu, D., and Raya, A. (2017). CRISPR/Cas9-based engineering of the epigenome. Cell Stem Cell *21*, 431–447. https://doi.org/10.1016/j.stem.2017.09.006.
38. Sokka, J., Yoshihara, M., Kvist, J., Laiho, L., Warren, A., Stadelmann, C., Jouhilahti, E.-M., Kilpinen, H., Balboa, D., Katayama, S., et al. (2022).

CRISPR activation enables high-fidelity reprogramming into human pluripotent stem cells. Stem Cell Rep. *17*, 413–426. https://doi.org/10.1016/j.stemcr.2021.12.017.

39. Niakan, K.K., Schrode, N., Cho, L.T.Y., and Hadjantonakis, A.-K. (2013). Derivation of extraembryonic endoderm stem (XEN) cells from mouse embryos and embryonic stem cells. Nat. Protoc. *8*, 1028–1041. https://doi.org/10.1038/nprot.2013.049.
40. Ralston, A., and Rossant, J. (2008). Cdx2 acts downstream of cell polarization to cell-autonomously promote trophectoderm fate in the early mouse embryo. Dev. Biol. *313*, 614–629. https://doi.org/10.1016/j.ydbio.2007.10.054.
41. Ralston, A., Cox, B.J., Nishioka, N., Sasaki, H., Chea, E., Rugg-Gunn, P., Guo, G., Robson, P., Draper, J.S., and Rossant, J. (2010). Gata3 regulates trophoblast development downstream of Tead4 and in parallel to Cdx2. Development *137*, 395–403. https://doi.org/10.1242/dev.038828.
42. Schrode, N., Saiz, N., Di Talia, S., and Hadjantonakis, A.-K. (2014). GATA6 levels modulate primitive endoderm cell fate choice and timing in the mouse blastocyst. Dev. Cell *29*, 454–467. https://doi.org/10.1016/j.devcel.2014.04.011.
43. Wamaitha, S.E., del Valle, I., Cho, L.T.Y., Wei, Y., Fogarty, N.M.E., Blakeley, P., Sherwood, R.I., Ji, H., and Niakan, K.K. (2015). Gata6 potently initiates reprograming of pluripotent and differentiated cells to extraembryonic endoderm stem cells. Genes Dev. *29*, 1239–1255. https://doi.org/10.1101/gad.257071.114.
44. Chowdhary, S., and Hadjantonakis, A.-K. (2022). Journey of the mouse primitive endoderm: from specification to maturation. Philos. Trans. R. Soc. Lond. B Biol. Sci. *377*, 20210252. https://doi.org/10.1098/rstb.2021.0252.
45. Qiao, Y., Ren, C., Huang, S., Yuan, J., Liu, X., Fan, J., Lin, J., Wu, S., Chen, Q., Bo, X., et al. (2020). High-resolution annotation of the mouse preimplantation embryo transcriptome using long-read sequencing. Nat. Commun. *11*, 2653. https://doi.org/10.1038/s41467-020-16444-w.
46. Gao, L., Wu, K., Liu, Z., Yao, X., Yuan, S., Tao, W., Yi, L., Yu, G., Hou, Z., Fan, D., et al. (2018). Chromatin accessibility landscape in human early embryos and its association with evolution. Cell *173*, 248–259.e15. https://doi.org/10.1016/j.cell.2018.02.028.
47. Berens, C., and Hillen, W. (2003). Gene regulation by tetracyclines. Constraints of resistance regulation in bacteria shape TetR for application in eukaryotes. Eur. J. Biochem. *270*, 3109–3121. https://doi.org/10.1046/j.1432-1033.2003.03694.x.
48. Morgani, S.M., Metzger, J.J., Nichols, J., Siggia, E.D., and Hadjantonakis, A.-K. (2018). Micropattern differentiation of mouse pluripotent stem cells recapitulates embryo regionalized cell fate patterning. eLife *7*, e32839. https://doi.org/10.7554/eLife.32839.
49. Christodoulou, N., Weberling, A., Strathdee, D., Anderson, K.I., Timpson, P., and Zernicka-Goetz, M. (2019). Morphogenesis of extra-embryonic tissues directs the remodelling of the mouse embryo at implantation. Nat. Commun. *10*, 3557. https://doi.org/10.1038/s41467-019-11482-5.
50. Knight, G.T., Lundin, B.F., Iyer, N., Ashton, L.M., Sethares, W.A., Willett, R.M., and Ashton, R.S. (2018). Engineering induction of singular neural rosette emergence within hPSC-derived tissues. eLife *7*, e37549. https://doi.org/10.7554/eLife.37549.
51. Sofroniew, N., Lambert, T., Bokota, G., Nunez-Iglesias, J., Sobolewski, P., Sweet, A., Gaifas, L., Evans, K., Burt, A., Doncila Pop, D., et al. (2025). napari: a multi-dimensional image viewer for Python (Zenodo). https://doi.org/10.5281/ZENODO.3555620.
52. Ulicna, K., Vallardi, G., Charras, G., and Lowe, A.R. (2021). Automated deep lineage tree analysis using a Bayesian single cell tracking approach. Front. Comput. Sci. *3*. https://doi.org/10.3389/fcomp.2021.734559.
53. Schmidt, U., Weigert, M., Broaddus, C., and Myers, G. (2018). Cell detection with star-convex polygons. Preprint at arXiv. https://doi.org/10.1007/978-3-030-00934-2_30.
54. Weigert, M., Schmidt, U., Haase, R., Sugawara, K., and Myers, G. (2020). Star-convex polyhedra for 3D object detection and segmentation in microscopy. In 2020 IEEE Winter Conference on Applications of Computer Vision (WACV) (IEEE). https://doi.org/10.1109/wacv45572.2020.9093435.
55. Zargari, A., Lodewijk, G.A., Mashhadi, N., Cook, N., Neudorf, C.W., Araghbidikashani, K., Hays, R., Kozuki, S., Rubio, S., Hrabeta-Robinson, E., et al. (2023). DeepSea is an efficient deep-learning model for single-cell segmentation and tracking in time-lapse microscopy. Cell Rep. Methods *3*, 100500. https://doi.org/10.1016/j.crmeth.2023.100500.
56. Moghe, P., Belousov, R., Ichikawa, T., Iwatani, C., Tsukiyama, T., Graner, F., Erzberger, A., and Hiiragi, T. (2023). Apical-driven cell sorting optimised for tissue geometry ensures robust patterning. Preprint at bioRxiv. https://doi.org/10.1101/2023.05.16.540918.
57. Latos, P.A., Sienerth, A.R., Murray, A., Senner, C.E., Muto, M., Ikawa, M., Oxley, D., Burge, S., Cox, B.J., and Hemberger, M. (2015). Elf5-centered transcription factor hub controls trophoblast stem cell self-renewal and differentiation through stoichiometry-sensitive shifts in target gene networks. Genes Dev. *29*, 2435–2448. https://doi.org/10.1101/gad.268821.115.
58. Lin, S.-C.J., Wani, M.A., Whitsett, J.A., and Wells, J.M. (2010). Klf5 regulates lineage formation in the pre-implantation mouse embryo. Development *137*, 3953–3963. https://doi.org/10.1242/dev.054775.
59. James, J.L., Hurley, D.G., Gamage, T.K.J.B., Zhang, T., Vather, R., Pantham, P., Murthi, P., and Chamley, L.W. (2015). Isolation and characterisation of a novel trophoblast side-population from first trimester placentae. Reproduction *150*, 449–462. https://doi.org/10.1530/REP-14-0646.
60. Huang, D., Guo, G., Yuan, P., Ralston, A., Sun, L., Huss, M., Mistri, T., Pinello, L., Ng, H.H., Yuan, G., et al. (2017). The role of Cdx2 as a lineage specific transcriptional repressor for pluripotent network during the first developmental cell lineage segregation. Sci. Rep. *7*, 17156. https://doi.org/10.1038/s41598-017-16009-w.
61. Qiu, C., Cao, J., Martin, B.K., Li, T., Welsh, I.C., Srivatsan, S., Huang, X., Calderon, D., Noble, W.S., Disteche, C.M., et al. (2022). Systematic reconstruction of cellular trajectories across mouse embryogenesis. Nat. Genet. *54*, 328–341. https://doi.org/10.1038/s41588-022-01018-x.
62. González-Velasco, Ó., Simon, M., Yilmaz, R., Parlato, R., Weishaupt, J., Imbusch, C.D., and Brors, B. (2024). Identifying similar populations across independent single cell studies without data integration. Preprint at bioRxiv. https://doi.org/10.1101/2024.09.27.615367.
63. Okubo, T., Rivron, N., Kabata, M., Masaki, H., Kishimoto, K., Semi, K., Nakajima-Koyama, M., Kunitomi, H., Kaswandy, B., Sato, H., et al. (2024). Hypoblast from human pluripotent stem cells regulates epiblast development. Nature *626*, 357–366. https://doi.org/10.1038/s41586-023-06871-2.
64. Chandrasekaran, A.P., and Li, M. (2024). Extra (embryonic) dialogues: keys to improved stem cell-based embryo models. Cell Stem Cell *31*, 155–157. https://doi.org/10.1016/j.stem.2024.01.004.
65. Jin, S., Plikus, M.V., and Nie, Q. (2024). CellChat for systematic analysis of cell-cell communication from single-cell transcriptomics. Nat. Protoc. *20*, 180–219. https://doi.org/10.1038/s41596-024-01045-4.
66. Goissis, M.D., Bradshaw, B., Posfai, E., and Rossant, J. (2023). Influence of FGF4 and BMP4 on FGFR2 dynamics during the segregation of epiblast and primitive endoderm cells in the pre-implantation mouse embryo. PLoS One *18*, e0279515. https://doi.org/10.1371/journal.pone.0279515.
67. Molotkov, A., and Soriano, P. (2018). Distinct mechanisms for PDGF and FGF signaling in primitive endoderm development. Dev. Biol. *442*, 155–161. https://doi.org/10.1016/j.ydbio.2018.07.010.
68. Graham, S.J.L., Wicher, K.B., Jedrusik, A., Guo, G., Herath, W., Robson, P., and Zernicka-Goetz, M. (2014). BMP signalling regulates the pre-implantation development of extra-embryonic cell lineages in the mouse embryo. Nat. Commun. *5*, 5667. https://doi.org/10.1038/ncomms6667.
69. Simon, C.S., Rahman, S., Raina, D., Schröter, C., and Hadjantonakis, A.-K. (2020). Live visualization of ERK activity in the mouse blastocyst

reveals lineage-specific signaling dynamics. Dev. Cell *55*, 341–353.e5. https://doi.org/10.1016/j.devcel.2020.09.030.

70. Artus, J., Panthier, J.-J., and Hadjantonakis, A.-K. (2010). A role for PDGF signaling in expansion of the extra-embryonic endoderm lineage of the mouse blastocyst. Development *137*, 3361–3372. https://doi.org/10.1242/dev.050864.

71. Klumpe, H.E., Langley, M.A., Linton, J.M., Su, C.J., Antebi, Y.E., and Elowitz, M.B. (2022). The context-dependent, combinatorial logic of BMP signaling. Cell Syst. *13*, 388–407.e10. https://doi.org/10.1016/j.cels.2022.03.002.

72. Cang, Z., Wang, Y., Wang, Q., Cho, K.W.Y., Holmes, W., and Nie, Q. (2021). A multiscale model via single-cell transcriptomics reveals robust patterning mechanisms during early mammalian embryo development. PLoS Comput. Biol. *17*, e1008571. https://doi.org/10.1371/journal.pcbi.1008571.

73. Maye, P., Becker, S., Kasameyer, E., Byrd, N., and Grabel, L. (2000). Indian hedgehog signaling in extraembryonic endoderm and ectoderm differentiation in ES embryoid bodies. Mech. Dev. *94*, 117–132. https://doi.org/10.1016/s0925-4773(00)00304-x.

74. Fan, R., Kim, Y.S., Wu, J., Chen, R., Zeuschner, D., Mildner, K., Adachi, K., Wu, G., Galatidou, S., Li, J., et al. (2020). Wnt/beta-catenin/Esrrb signalling controls the tissue-scale reorganization and maintenance of the pluripotent lineage during murine embryonic diapause. Nat. Commun. *11*, 5499. https://doi.org/10.1038/s41467-020-19353-0.

75. Xia, J., Swiercz, J.M., Bañón-Rodríguez, I., Matković, I., Federico, G., Sun, T., Franz, T., Brakebusch, C.H., Kumanogoh, A., Friedel, R.H., et al. (2015). Semaphorin-plexin signaling controls mitotic spindle orientation during epithelial morphogenesis and repair. Dev. Cell *33*, 299–313. https://doi.org/10.1016/j.devcel.2015.02.001.

76. Thowfeequ, S., Fiorentino, J., Hu, D., Solovey, M., Ruane, S., Whitehead, M., Zhou, F., Godwin, J., Mateo-Otero, Y., Vanhaesebroeck, B., et al. (2024). An integrated approach identifies the molecular underpinnings of murine anterior visceral endoderm migration. Dev. Cell *59*, 2347–2363.e9. https://doi.org/10.1016/j.devcel.2024.05.014.

77. Io, S., Kabata, M., Iemura, Y., Semi, K., Morone, N., Minagawa, A., Wang, B., Okamoto, I., Nakamura, T., Kojima, Y., et al. (2021). Capturing human trophoblast development with naive pluripotent stem cells in vitro. Cell Stem Cell *28*, 1023–1039.e13. https://doi.org/10.1016/j.stem.2021.03.013.

78. Ng, R.K., Dean, W., Dawson, C., Lucifero, D., Madeja, Z., Reik, W., and Hemberger, M. (2008). Epigenetic restriction of embryonic cell lineage fate by methylation of Elf5. Nat. Cell Biol. *10*, 1280–1290. https://doi.org/10.1038/ncb1786.

79. Hemberger, M., Udayashankar, R., Tesar, P., Moore, H., and Burton, G.J. (2010). ELF5-enforced transcriptional networks define an epigenetically regulated trophoblast stem cell compartment in the human placenta. Hum. Mol. Genet. *19*, 2456–2467. https://doi.org/10.1093/hmg/ddq128.

80. Bedzhov, I., Bialecka, M., Zielinska, A., Kosalka, J., Antonica, F., Thompson, A.J., Franze, K., and Zernicka-Goetz, M. (2015). Development of the anterior-posterior axis is a self-organizing process in the absence of maternal cues in the mouse embryo. Cell Res. *25*, 1368–1371. https://doi.org/10.1038/cr.2015.104.

81. Yurchenco, P.D., Amenta, P.S., and Patton, B.L. (2004). Basement membrane assembly, stability and activities observed through a developmental lens. Matrix Biol. *22*, 521–538. https://doi.org/10.1016/j.matbio.2003.10.006.

82. Miner, J.H., Li, C., Mudd, J.L., Go, G., and Sutherland, A.E. (2004). Compositional and structural requirements for laminin and basement membranes during mouse embryo implantation and gastrulation. Development *131*, 2247–2256. https://doi.org/10.1242/dev.01112.

83. Aszódi, A., Legate, K.R., Nakchbandi, I., and Fässler, R. (2006). What mouse mutants teach us about extracellular matrix function. Annu. Rev. Cell Dev. Biol. *22*, 591–621. https://doi.org/10.1146/annurev.cellbio.22.010305.104258.

84. Futaki, S., Nakano, I., Kawasaki, M., Sanzen, N., and Sekiguchi, K. (2019). Molecular profiling of the basement membrane of pluripotent epiblast cells in post-implantation stage mouse embryos. Regen. Ther. *12*, 55–65. https://doi.org/10.1016/j.reth.2019.04.010.

85. Kyprianou, C., Christodoulou, N., Hamilton, R.S., Nahaboo, W., Boomgaard, D.S., Amadei, G., Migeotte, I., and Zernicka-Goetz, M. (2020). Basement membrane remodelling regulates mouse embryogenesis. Nature *582*, 253–258. https://doi.org/10.1038/s41586-020-2264-2.

86. Stephenson, R.O., Yamanaka, Y., and Rossant, J. (2010). Disorganized epithelial polarity and excess trophectoderm cell fate in preimplantation embryos lacking E-cadherin. Development *137*, 3383–3391. https://doi.org/10.1242/dev.050195.

87. Bedzhov, I., and Zernicka-Goetz, M. (2014). Self-organizing properties of mouse pluripotent cells initiate morphogenesis upon implantation. Cell *156*, 1032–1044. https://doi.org/10.1016/j.cell.2014.01.023.

88. Rugg-Gunn, P.J., Moris, N., and Tam, P.P.L. (2023). Technical challenges of studying early human development. Development *150*, dev201797. https://doi.org/10.1242/dev.201797.

89. Saiz, N., Mora-Bitria, L., Rahman, S., George, H., Herder, J.P., Garcia-Ojalvo, J., and Hadjantonakis, A.-K. (2020). Growth-factor-mediated coupling between lineage size and cell fate choice underlies robustness of mammalian development. eLife *9*, e56079. https://doi.org/10.7554/eLife.56079.

90. Vasiev, B., Balter, A., Chaplain, M., Glazier, J.A., and Weijer, C.J. (2010). Modeling gastrulation in the chick embryo: formation of the primitive streak. PLoS One *5*, e10571. https://doi.org/10.1371/journal.pone.0010571.

91. Tanner, K., Mori, H., Mroue, R., Bruni-Cardoso, A., and Bissell, M.J. (2012). Coherent angular motion in the establishment of multicellular architecture of glandular tissues. Proc. Natl. Acad. Sci. USA *109*, 1973–1978. https://doi.org/10.1073/pnas.1119578109.

92. Yanagida, A., Corujo-Simon, E., Revell, C.K., Sahu, P., Stirparo, G.G., Aspalter, I.M., Winkel, A.K., Peters, R., De Belly, H., Cassani, D.A.D., et al. (2022). Cell surface fluctuations regulate early embryonic lineage sorting. Cell *185*, 1258. https://doi.org/10.1016/j.cell.2022.03.015.

93. Sato, N., Rosa, V.S., Makhlouf, A., Kretzmer, H., Sampath Kumar, A., Grosswendt, S., Mattei, A.L., Courbot, O., Wolf, S., Boulanger, J., et al. (2024). Basal delamination during mouse gastrulation primes pluripotent cells for differentiation. Dev. Cell *59*, 1252–1268.e13. https://doi.org/10.1016/j.devcel.2024.03.008.

94. Karzbrun, E., Khankhel, A.H., Megale, H.C., Glasauer, S.M.K., Wyle, Y., Britton, G., Warmflash, A., Kosik, K.S., Siggia, E.D., Shraiman, B.I., et al. (2021). Human neural tube morphogenesis in vitro by geometric constraints. Nature *599*, 268–272. https://doi.org/10.1038/s41586-021-04026-9.

95. Magnusson, J.P., Rios, A.R., Wu, L., and Qi, L.S. (2021). Enhanced Cas12a multi-gene regulation using a CRISPR array separator. eLife *10*, e66406. https://doi.org/10.7554/eLife.66406.

96. Kempton, H.R., Goudy, L.E., Love, K.S., and Qi, L.S. (2020). Multiple input sensing and signal integration using a split Cas12a system. Mol. Cell *78*, 184–191.e3. https://doi.org/10.1016/j.molcel.2020.01.016.

97. van der Walt, S., Schönberger, J.L., Nunez-Iglesias, J., Boulogne, F., Warner, J.D., Yager, N., Gouillart, E., and Yu, T.; Scikit-Image Contributors (2014). scikit-image: image processing in Python. PeerJ *2*, e453. https://doi.org/10.7717/peerj.453.

98. Wickham, H. (2016). Ggplot2, Second edition (Springer International Publishing).

99. Wortel, I.M.N., Liu, A.Y., Dannenberg, K., Berry, J.C., Miller, M.J., and Textor, J. (2021). CelltrackR: an R package for fast and flexible analysis of immune cell migration data. Immunoinformatics (Amst.) *1–2*, 100003. https://doi.org/10.1016/j.immuno.2021.100003.

100. Schindelin, J., Arganda-Carreras, I., Frise, E., Kaynig, V., Longair, M., Pietzsch, T., Preibisch, S., Rueden, C., Saalfeld, S., Schmid, B., et al.

(2012). Fiji: an open-source platform for biological-image analysis. Nat. Methods *9*, 676–682. https://doi.org/10.1038/nmeth.2019.

101. Goedhart, J. (2020). PlotTwist: A web app for plotting and annotating continuous data. PLoS Biol. *18*, e3000581. https://doi.org/10.1371/journal.pbio.3000581.
102. Melsted, P., Booeshaghi, A.S., Liu, L., Gao, F., Lu, L., Min, K.H.J., da Veiga Beltrame, E., Hjörleifsson, K.E., Gehring, J., and Pachter, L. (2021). Modular, efficient and constant-memory single-cell RNA-seq preprocessing. Nat. Biotechnol. *39*, 813–818. https://doi.org/10.1038/s41587-021-00870-2.
103. Hao, Y., Stuart, T., Kowalski, M.H., Choudhary, S., Hoffman, P., Hartman, A., Srivastava, A., Molla, G., Madad, S., Fernandez-Granda, C., et al. (2024). Dictionary learning for integrative, multimodal and scalable single-cell analysis. Nat. Biotechnol. *42*, 293–304. https://doi.org/10.1038/s41587-023-01767-y.
104. Wang, Z., and Jaenisch, R. (2004). At most three ES cells contribute to the somatic lineages of chimeric mice and of mice produced by ES-tetraploid complementation. Dev. Biol. *275*, 192–201. https://doi.org/10.1016/j.ydbio.2004.06.026.
105. Chavez, A., Scheiman, J., Vora, S., Pruitt, B.W., Tuttle, M., P R Iyer, E., Lin, S., Kiani, S., Guzman, C.D., Wiegand, D.J., et al. (2015). Highly efficient Cas9-mediated transcriptional programming. Nat. Methods *12*, 326–328. https://doi.org/10.1038/nmeth.3312.
106. Lee, J.Y., Chang, J.K., Dominguez, A.A., Lee, H.-P., Nam, S., Chang, J., Varma, S., Qi, L.S., West, R.B., and Chaudhuri, O. (2019). YAP-independent mechanotransduction drives breast cancer progression. Nat. Commun. *10*, 1848. https://doi.org/10.1038/s41467-019-09755-0.
107. Chiu, C.L., and Clack, N. (2022). napari: a Python Multi-Dimensional Image Viewer Platform for the Research Community. Microsc. Microanal. *28*, 1576–1577. https://doi.org/10.1017/s1431927622006328.
108. Concordet, J.-P., and Haeussler, M. (2018). CRISPOR: intuitive guide selection for CRISPR/Cas9 genome editing experiments and screens. Nucleic Acids Res. *46*, W242–W245. https://doi.org/10.1093/nar/gky354.
109. Galaxy Community (2024). The Galaxy platform for accessible, reproducible, and collaborative data analyses: 2024 update. Nucleic Acids Res. *52*, W83–W94. https://doi.org/10.1093/nar/gkae410.
110. Bolger, A.M., Lohse, M., and Usadel, B. (2014). Trimmomatic: a flexible trimmer for Illumina sequence data. Bioinformatics *30*, 2114–2120. https://doi.org/10.1093/bioinformatics/btu170.
111. Langmead, B., and Salzberg, S.L. (2012). Fast gapped-read alignment with Bowtie 2. Nat. Methods *9*, 357–359. https://doi.org/10.1038/nmeth.1923.
112. Ramírez, F., Ryan, D.P., Grüning, B., Bhardwaj, V., Kilpert, F., Richter, A.S., Heyne, S., Dündar, F., and Manke, T. (2016). deepTools2: a next generation web server for deep-sequencing data analysis. Nucleic Acids Res. *44*, W160–W165. https://doi.org/10.1093/nar/gkw257.
113. Kim, D., Langmead, B., and Salzberg, S.L. (2015). HISAT: a fast spliced aligner with low memory requirements. Nat. Methods *12*, 357–360. https://doi.org/10.1038/nmeth.3317.
114. Liao, Y., Smyth, G.K., and Shi, W. (2014). featureCounts: an efficient general purpose program for assigning sequence reads to genomic features. Bioinformatics *30*, 923–930. https://doi.org/10.1093/bioinformatics/btt656.
115. Perez, G., Barber, G.P., Benet-Pages, A., Casper, J., Clawson, H., Diekhans, M., Fischer, C., Gonzalez, J.N., Hinrichs, A.S., Lee, C.M., et al. (2025). The UCSC Genome Browser database: 2025 update. Nucleic Acids Res. *53*, D1243–D1249. https://doi.org/10.1093/nar/gkae974.

Please cite this article in press as: Lodewijk et al., Self-organization of mouse embryonic stem cells into reproducible pre-gastrulation embryo models via CRISPRa programming, Cell Stem Cell (2025), https://doi.org/10.1016/j.stem.2025.02.015

STAR★METHODS

KEY RESOURCES TABLE

REAGENT or RESOURCE	SOURCE	IDENTIFIER
Antibodies		
See Table S3	This study	N/A
Rabbit monoclonal anti-Cdx2	Cell Signaling Technology	Cat#12306; RRID: AB_2797879
Rabbit monoclonal anti-Gata6	Cell Signaling Technology	Cat#5851; RRID: AB_10705521
Rabbit monoclonal anti-Gata3	Cell Signaling Technology	Cat#5852; RRID: AB_10835690
Goat polyclonal anti-Tfap2c	R&D Systems	Cat#AF5059; RRID: AB_2255891
Mouse monoclonal anti-Foxa1	Abcam	Cat#ab55178; RRID: AB_941631
Goat polyclonal anti-Sox17	R&D Systems	Cat#AF1924; RRID: AB_355060
Goat polyclonal anti-Oct3/4	R&D Systems	Cat#AF1759; RRID: AB_354975
Mouse monoclonal anti-Oct3/4	Santa Cruz Biotechnology	Cat#sc-5279; RRID: AB_628051
Rabbit monoclonal anti-Oct4a	Cell Signaling Technology	Cat#2840; RRID: AB_2167691
Rabbit monoclonal anti-Nanog	Cell Signaling Technology	Cat#4903; RRID: AB_10559205
Goat polyclonal anti-Lefty1	R&D Systems	Cat#AF746; RRID: AB_355566
Rat polyclonal anti-Cer1	R&D Systems	Cat# MAB1986; RRID: AB_2275974
Goat polyclonal anti-Dkk1	R&D Systems	Cat#AF1096; RRID: AB_354597
Rat monoclonal anti-Lama1	R&D Systems	Cat#MAB4656; RRID: AB_2265518
Goat polyclonal anti-Cdh1	R&D Systems	Cat#AF748; RRID: AB_355568
Goat polyclonal anti-Pdgfra	R&D Systems	Cat#AF1062; RRID: AB_2236897
Mouse monoclonal anti-Lim1	R&D Systems	Cat#MAB2725; RRID: AB_2135636
Donkey polyclonal anti-Goat Alexa 488	Thermo Fisher Scientific	Cat#A-11055; RRID: AB_2534102
Goat polyclonal anti-Mouse Alexa 488	Thermo Fisher Scientific	Cat#A-11001; RRID: AB_2534069
Donkey polyclonal anti-Rabbit Alexa 488	Thermo Fisher Scientific	Cat#A-21206; RRID: AB_2535792
Donkey polyclonal anti-Mouse Alexa 568	Thermo Fisher Scientific	Cat#A-10037; RRID: AB_11180865
Donkey polyclonal anti-Rabbit Alexa 594	Thermo Fisher Scientific	Cat#A-21207; RRID: AB_141637
Goat polyclonal anti-Mouse Alexa 594	Thermo Fisher Scientific	Cat#A-11005; RRID: AB_2534073
Donkey polyclonal anti-Rat Alexa 647	Thermo Fisher Scientific	Cat#A-48272; RRID: AB_2893138
Donkey polyclonal anti-Goat Alexa 647	Thermo Fisher Scientific	Cat#A-21447; RRID: AB_2535864
Donkey polyclonal anti-Goat Plus Alexa 647	Thermo Fisher Scientific	Cat#A-32849; RRID: AB_2762840
Bacterial and virus strains		
DH5a competent E. coli	New England Biolabs	Cat#C2987H
NEB Stable competent E. coli	New England Biolabs	Cat#3040H
Chemicals, peptides, and recombinant proteins		
ESGRO-2i medium	MilliporeSigma	Cat#SF016-200
PD0325901	StemRD	Cat#PD-010
ESC Qualified FBS	MilliporeSigma	Cat#ES-009-B
CHIR99021	StemRD	Cat#CHIR-010
Leukemia inhibitory factor	MilliporeSigma	Cat#ESG1107
Doxycycline	MilliporeSigma	Cat#D5207
rhLaminin-521	Thermo Fisher Scientific	Cat#A29248
ROCK inhibitor	STEMCELL Technologies	Cat#72304
Lipofectamine™ Stem Transfection Reagent	Thermo Fisher Scientific	Cat#STEM00003
TurboFect™ Transfection Reagent	Thermo Fisher Scientific	Cat#R0531
Hygromycin	Mirus Bio	Cat#MIR5930
Puromycin	STEMCELL Technologies	Cat#73342

(*Continued on next page*)

Please cite this article in press as: Lodewijk et al., Self-organization of mouse embryonic stem cells into reproducible pre-gastrulation embryo models via CRISPRa programming, Cell Stem Cell (2025), https://doi.org/10.1016/j.stem.2025.02.015

CellPress
OPEN ACCESS

Continued

REAGENT or RESOURCE	SOURCE	IDENTIFIER
Critical commercial assays		
Single-cell RNA-seq Service, 10X Genomics V3	Novogene Corporation Inc.	N/A
Deposited data		
CPEM scRNAseq data	This study	GEO: GSE256138
Codes used to process scRNA-Seq data	This study	https://doi.org/10.5281/zenodo.14511168
ETX model scRNAseq data	Dupont et al.[28]	GEO: GSE206132
E5.25 embryo scRNAseq data	Qiu et al.[61]	GEO: GSE109071
mESC Cdx2 cDNA overexpression RNAseq data	Tarazi et al.[2]	GEO: GSE208681
Blastocyst RNAseq data	Qiao et al.[45]	ENA: PRJNA577068
Blastocyst DNAseI hypersensitivity data	Gao et al.[46]	NGDC GSA: CRA000297
Experimental models: Cell lines		
Mouse ESC V6.5	Wang and Jaenisch[104]	RRID:CVCL_C865
HEK293T	ATCC	Cat#CRL-3216; RRID:CVCL_0063
sgCtrl-mESC	This study	N/A
sgGata6-mESC	This study	N/A
sgCdx2-mESC	This study	N/A
sgCdx2+sgElf5-mESC	This study	N/A
sgCtrl-mTagBFP-NLS-mESC	This study	N/A
sgGata6-mCherry-NLS-mESC	This study	N/A
sgCdx2-Clover-NLS-mESC	This study	N/A
sgLama1-mESC	This study	N/A
sgMmp2-mESC	This study	N/A
sgMmp14-mESC	This study	N/A
Oligonucleotides		
See Table S2	This study	N/A
Recombinant DNA		
PB-TRE3G-dCas9-VPR cassette	Chavez et al.[105]	Addgene Cat#63800
PiggyBac Transposase	System Biosciences	Cat#PB210PA-1
pUC19	New England Biolabs	Cat#N3041S
pSLQ1371-sgRNA cassette	Lee et al.[106]	Addgene Cat#121425
VSVG	Trono lab	Addgene Cat#12259
DR8.74	Trono lab	Addgene Cat#22036
Software and algorithms		
Gen5 software (3.14)	Agilent BioTek	https://www.agilent.com/en/support/biotek-software-releases
Zeiss ZEN software	ZEISS	https://www.zeiss.com/microscopy/us/products/software/zeiss-zen.html
Fusion Benchtop software	Andor Technology Ltd, Oxford Instruments	https://andor.oxinst.com/downloads/view/fusion-1.1.1-for-bc43
imageJ (Fiji) (1.54f)	Schindelin et al.[100]	https://imagej.net/Fiji
R (4.4.2)	R Foundation for Statistical Computing	https://www.r-project.org/
Rstudio (2024.09.1)	RStudio Team (2020)	https://www.rstudio.com/
Napari (0.4.18)	Chiu and Clack[107]	https://napari.org/stable/
Stardist (stardist-napari 2022.12.6)	Weigert et al.[54]	https://github.com/stardist/stardist-napari
RegionProps (napari-skimage-regionprops 0.10.1)	van der Walt et al.[97]	https://scikit-image.org/
Btrack (0.6.4)	Ulicna et al.[52]	https://github.com/quantumjot/btrack
wizard (napari-animation 0.0.7)	Napari	https://github.com/napari/napari-animation
celltrackR (1.1.0)	Wortel et al.[99]	https://github.com/ingewortel/celltrackR

(*Continued on next page*)

Continued

REAGENT or RESOURCE	SOURCE	IDENTIFIER
ggplot2	Wickham[98]	https://ggplot2.tidyverse.org/
ggridges	Wilke Lab	https://wilkelab.org/ggridges/
PlotTwist	Goedhart[101]	https://github.com/JoachimGoedhart/PlotTwist
CRISPOR	Concordet and Haeussler[108]	https://github.com/maximilianh/crisporWebsite
Galaxy Project	The Galaxy Community[109]	https://usegalaxy.org/
Trimmomatic (0.39+galaxy2)	Bolger et al.[110]	https://github.com/timflutre/trimmomatic
Bowtie2 (2.5.3+galaxy1)	Langmead and Salzberg[111]	https://github.com/BenLangmead/bowtie2
deepTools (3.5.4+galaxy0)	Ramirez et al.[112]	https://github.com/deeptools/deepTools
HISAT2 (2.2.1+galaxy1)	Kim et al.[113]	https://github.com/DaehwanKimLab/hisat2
Featurecounts (2.0.8+galaxy0)	Liao et al.[114]	https://rnnh.github.io/bioinfo-notebook/docs/featureCounts.html
UCSC Genome Browser	Perez et al.[115]	https://genome.ucsc.edu/
kallisto-bustools (kb_python-0.28.2)	Melsted et al.[102]	https://www.kallistobus.tools/
Seurat (5.0.1)	Hao et al.[103]	https://github.com/satijalab/seurat/
CellChat v2 (2.1.1)	Jin et al.[65]	https://github.com/sqjin/CellChat
ClusterFoldSimilarity	González-Velasco et al.[62]	https://github.com/OscarGVelasco/ClusterFoldSimilarity
Other		
CYTOO™ Arena A x18	CYTOO	Cat#10-020-00-18
Spinal 6-Well 100μm RosetteArray™ Plate	Neurosetta	N/A
AggreWell 400	STEMCELL Technologies	Cat#34415
Anti-adherence solution	STEMCELL Technologies	Cat#07010
Falcon™ Cell Strainers	Corning	Cat#087711
15mm Netwell™ Insert with 74μm Mesh Size Polyester Membrane	Corning	Cat#3477
μ-Slide 8 Well Glass Bottom	Ibidi	Cat#80827
Glycerol	MilliporeSigma	Cat#G2025
Clear nail polish	Ted Pella	Cat#114-7
Oxford Instruments Andor BC-43	Oxford Instruments	N/A
Lionheart FX microscope	Agilent BioTek	N/A
Zeiss 880 Confocal microscope	ZEISS	N/A
Andor BC43 Confocal microscope	Andor Technology Ltd, Oxford Instruments	N/A

EXPERIMENTAL MODEL AND STUDY PARTICIPANT DETAILS

Cell lines

Mouse (male) v6.5 embryonic stem cells (mESCs) (RRID:CVCL_C865) were cultured in 2i+Lif conditions in either ESGRO-2i medium (MilliporeSigma, SF016-200) +1x Pen/Strep (Thermo Fisher Scientific, 15140122) or N2B27 medium (Takara, Y40002) supplemented with 1x Pen/Strep (Thermo Fisher Scientific, 15140122), 1uM PD0325901 (StemRD, PD-010), 3uM CHIR99021 (StemRD, CHIR-010) and 1000 U/ml Lif (MilliporeSigma, ESG1107). mESCs were grown on tissue culture treated plates coated with 0.1% gelatin (Sigma G1890). For routine passaging, cells were seeded at 5,000-10,000 cells per cm^2 and passaged every 2-3 days using Accutase (Innovative Cell Technologies, AT104). Cells were grown in humidified incubators at 37°C, 5% CO2 and ambient O2.

Human HEK293T (female) (RRID:CVCL_0063) cells were grown in DMEM+Glutamax (Thermo Fisher Scientific, 10566024), 1x Pen/Strep (Thermo Fisher Scientific, 15140122) and 10% HIFBS (Thermo Fisher Scientific, 10438026), on tissue culture treated plates. For maintaining cultures, cells were split using 0.25% Trypsin + 0.5mM EDTA (Thermo Fisher Scientific, 25200072) every 3-4 days at a subcultivation ratio of 1/10. Cells were grown in humidified incubators at 37°C, 5% CO2 and ambient O2.

METHOD DETAILS

ChIP-sequencing data analysis

Raw fastq files were downloaded from sequence data repositories (NGDC GSA CRA000297) and imported to Galaxy. Files were trimmed using Trimmomatic using the following settings: SLIDINGWINDOW: window=4, qual=20 and MINLEN: 30. The Illuminaclip

command was specified when necessary to remove adapters from reads. Reads were mapped to mm10 reference genome using Bowtie2 with the very sensitive end-to-end preset. BAM files were converted to Bigwig files for visualization on the UCSC Genome Browser with deepTools bamCoverage, bin size 1, without normalizing or scaling.

RNA-sequencing data analysis

Raw fastq files were downloaded from sequence data repositories (ENA PRJNA577068) and imported to Galaxy. Fastq files were trimmed using Trimmomatic with parameters ''ILLUMINACLIP: Truseq v3, SLIDINGWINDOW: window=4, qual=20 and MINLEN: 30''. Reads passing QC were mapped onto the mm10 reference genome using HISAT2. Raw read counts were generated with featurecounts. Coverage tracks in bigwig format were made using deepTools bamCoverage with settings ''bin size 1, do not normalize or scale, ignore missing data, minimum mapping quality 1. Bigwig files were visualized on the UCSC Genome Browser and scaled according to total read count per sample.

Introduction of the inducible CRISPRa cassette

For integrating the PB-TRE3G-dCas9-VPR cassette (dCas9-VPR) (Addgene, #63800), cells were transfected using Lipofectamine Stem (Thermo Fisher Scientific, STEM00003), diluted in OptiMEM (Thermo Fisher, 31985062). Briefly, mESCs were seeded in 0.1% gelatin coated 6 well plates as described before, seeding 300,000 cells per well. The next day, cells were transfected with the following plasmids diluted in OptiMEM: 200 ng PiggyBac Transposase (SBI, PB210PA-1), 800 ng PB-TRE3G-dCas-VPR (Addgene, 63800) and 1000 ng pUC19 (NEB, N3041S). As a non-integrating control transfection, the following condition was used: PB-TRE3G-dCas-VPR (800 ng) and pUC19 (1200 ng). Medium was replaced 6 hours after transfection. 48 hours after transfection, cells with successful integration were selected by addition of 100 μg/ml Hygromycin (Mirus Bio, MIR5930) for 4 days, or until no control cells were remaining.

Lentiviral transduction of sgRNA cassettes

The pSLQ1371-sgRNA cassette (Addgene, 121425) was integrated via lentiviral transduction. To prepare lentivirus, HEK293T cells were seeded on 6 well plates at a density of 500,000 cells per well, in medium consisting of DMEM+Glutamax (Thermo Fisher Scientific, 10566024), 1x Pen/Strep (Thermo Fisher Scientific, 15140122) and 10% HIFBS (Thermo Fisher Scientific, 10438026). The next day, per well, medium was replaced to 2ml DMEM+Glutamax (Thermo Fisher Scientific 10566024) and 10% ESC qualified FBS (MilliporeSigma, ES-009-B). Cells were then transfected using Turbofect (Thermo Fisher Scientific, R0531) with the following plasmids: 300 ng VSVG (Addgene, 12259), 450 ng DR8.74 (Addgene, 22036), 750 ng pSLQ1371-sgRNA (Addgene, 121425). 6-24 hours after transfection, 1 ml DMEM+Glutamax (Thermo Fisher Scientific, 10566024), 3x Pen/Strep (final concentration 1x) (Thermo Fisher Scientific, 15140122), and 10% ESC qualified FBS (MilliporeSigma, ES-009-B) was added. Lentivirus was harvested 72 hours after transfection by collecting the medium into tubes, followed by centrifugation at 500 rcf. Next, the supernatant was filtered through a 0.45 μm filter (MilliporeSigma, SLHVM33RS) and collected into new tubes.

For lentiviral transduction, mESCs were seeded on 0.1% gelatin coated 6 well plates at a density of 50,000 cells per well. The next day, medium was replaced with 1 ml 2i+Lif medium and 1 ml prepared lentivirus. After 24 hours of incubating the lentivirus, medium was replaced again to 2i+Lif only medium. To select for transduced cells, 0.8 μg/ml Puromycin (Stemcell Technologies, 73342) was added 48 hours after lentiviral transduction, and added for 4 days or until no control cells (non-transduced cells) were remaining.

Using the above methods, the 3 mESC lines were generated with a control non-targeting gRNA, Gata6 targeting gRNA and Cdx2 targeting gRNA[97] (Figure S1A), for initial model establishment, and additional gRNAs targeting Elf5, Lama1, Mmp2 and Mmp14 were generated (Table S2)

To generate the dual sgCdx2+sgElf5 mESC line, the sgCdx2-Clover-NLS mESC line was transduced again with lentivirus encoding for sgElf5-mCherry. Dual-transduced cells were selected using fluorescence activated cell sorting (FACS) by collecting Clover+/mCherry+ double positive cells. Collected cells were centrifuged for 5 minutes at 200rcf, replated and grown in 2i+lif conditions as described previously.

CRISPRa validation immunofluorescence staining

For validation of the sgCtrl, sgCdx2 and sgGata6 mESC CRISPRa lines, induction of target genes was done by immunofluorescence staining. mESCs were seeded 0.1% gelatin coated 24 well plates. Depending on experiment duration, cells were seeded at the following densities: 24 hour treatment - 50,000 cells per well, 48 hour treatment - 25,000 cells per well, 72 hour treatment - 12,500 cells per well, 96 hour treatment - 6,250 cells per well. For each staining sgCtrl-mESC, sgGata6-mESC and sgCdx2-mESC were seeded in duplicate to perform doxycycline and no doxycycline control treatments. Cells were seeded in standard differentiation medium: DMEM+Glutamax, 15% ESC qualified FBS, 1x Sodium Pyruvate (Thermo Fisher, 11360070), 1x Non-essential amino acids (Thermo Fisher, 11140050), 1x Pen/Strep and 0.1 mM beta-mercaptoethanol (Thermo Fisher, 21985023). Doxycycline was added at 0.5 μg/ml (Millipore Sigma, D5207) in treatment wells. Medium was changed every 24 hours until ready for immunofluorescence staining. Cells were prepared by adding 0.4 ml of 3.6% Formaldehyde (Avantor, JTS898-7) in 1x PBS and incubating for 10 minutes at room temperature. Each well was washed twice with 1x PBS and incubated with 0.2% Triton-X100 (VWR, 97063-864) in 1x PBS for 20 minutes. Each well was washed once with 1x PBS and incubated with 0.4 ml Blocking buffer consisting of 3% BSA + 0.1% Triton in 1x PBS (Blocking buffer) for 1 hour. Blocking buffer was removed, 0.4 ml of Primary antibody incubation solution was added per well, consisting of 1% BSA in 1x PBS and primary antibodies (Table S3). Plates were incubated overnight at 4°C.

Please cite this article in press as: Lodewijk et al., Self-organization of mouse embryonic stem cells into reproducible pre-gastrulation embryo models via CRISPRa programming, Cell Stem Cell (2025), https://doi.org/10.1016/j.stem.2025.02.015

The next day, Primary antibody incubation solution was removed and wells were washed twice with 0.1% Tween in 1x PBS and washed once with 1x PBS. 0.4 ml of Secondary antibody solution was used, consisting of 1% BSA in 1x PBS and secondary antibodies (Table S3). Plates were incubated at room temperature for 1 hour. Secondary antibody solution was removed and wells were incubated with 0.5 μg/ml DAPI + 0.1% Tween (BioRad,1610781) in 1x PBS for 5 minutes. Wells were washed once with 0.1% Tween in 1x PBS and twice with 1x PBS. For imaging, 0.5 ml of 1x PBS was added per well. All washing steps were 3 minutes each and approximately 0.5 ml volume unless otherwise indicated.

CRISPRa validation analysis

Immunofluorescence and phase contrast images were captured using the Lionheart FX system (Agilent BioTek) with Gen5 software (3.14). 16 images were captured per well, using phase contrast, DAPI, GFP and TexasRed channels. Images were processed in imageJ. Image stacks were loaded per channel and a binary mask was created using DAPI stain for each condition, to identify individual nuclei regions. Then, the DAPI mask was used to measure intensity of stainings in GFP and TexasRed channels. The mean intensity per nucleus for each staining was extracted in this way for all conditions and plotted using the ggplot2[98] and ggridges packages in Rstudio. The number of positive and negative cells was calculated by setting a threshold value.

Micropattern culture and immunofluorescence staining

For micropattern culture and end-point immunofluorescence staining, Cytoo Arena A microchips (CYTOO, 10-020-00-18) were used. Chips were placed into 6 well plates already containing 3 ml of 1x PBS. Then, 1x PBS was removed and 3 ml of 4 μg/ml Laminin in 1x PBS was added and placed in a cell culture incubator for 2 hours at 37°C, 5% CO2. Wells were washed by adding 6 ml 1x PBS per well and removing 6 ml solution, repeated 5 times. Then, one well at a time, complete solution was removed and 3 ml 2i+Lif medium + 10uM ROCK inhibitor (Stemcell Technologies, 72304) was added. Plates were placed in the incubator until needed the same day. To plate cells, sgCtrl-mESCs, sgGata6-mESCs and sgCdx2-mESCs were individually collected, counted, and mixed together in a 1:1:1 ratio. Then, 120,000 cells were added per well (40,000 for each line). After 2 hours, medium was replaced to standard differentiation medium: DMEM+Glutamax, 15% ESC qualified FBS, 1x Sodium Pyruvate, 1x Non-essential amino acids, 1x Pen/Strep and 0.1 mM beta-mercaptoethanol, and doxycycline was added to treatment wells. Medium was changed daily, one well at a time. Cells were grown on microchips for 72 hours before immunofluorescence staining.

To prepare Cytoo Arena A microchips for immunostaining, medium was removed and wells were washed once with 1x PBS, followed by addition of 3 ml 3.6% formaldehyde in 1x PBS per well and incubated 30 minutes at room temperature. Each well was washed twice with 1x PBS and microchips were transferred from 6 well plates into individual 35mm plates per microchip, already containing 3 ml 1x PBS. The solution was replaced with 3 ml 0.2% Triton in 1x PBS and incubated for 30 minutes at room temperature. Each dish was washed once with 1x PBS and incubated with 3 ml Blocking buffer consisting of 3% BSA + 0.1% Triton in 1x PBS (Blocking buffer) for 2 hours. Blocking buffer was removed, 2.5 ml of Primary antibody incubation solution was added per dish, consisting of 1% BSA in 1x PBS, including diluted antibodies to a concentration of 1-2 μg/ml each (Table S3). Dishes were incubated overnight at 4°C.

The next day, Primary antibody incubation solution was removed and dishes were washed twice with 0.1% Tween in 1x PBS and washed once with 1x PBS. Dishes were incubated for 2 hours at room temperature in 2.5 ml of Secondary antibody solution, consisting of 1% BSA in 1x PBS, including diluted secondary antibodies (Table S3). Secondary antibody solution was removed and dishes were incubated with 0.5 μg/ml DAPI + 0.1% Tween in 1x PBS for 10 minutes. Dishes were washed once with 0.1% Tween in 1x PBS and twice with 1x PBS. For imaging, 3 ml of 1x PBS was added per dish. All washing steps were 5 minutes each and 1 ml volume unless otherwise indicated. Immunofluorescence images were captured using the Zeiss LSM880 confocal laser scanning microscope system.

Micropattern image segmentation and processing

For each channel, tiled image scans were stitched, followed by maximum projection intensity of z-stacks (11 image stack, 3.19um z-intervals), in Zeiss ZEN software. The resulting images were imported into Napari per channel and segmented using StarDist (stardist-napari 2022.12.6). The following settings were used: Model Type: 2D. Pre-trained model: Versatile (fluorescent nuclei). Normalize image yes, percentile low = 1.00, percentile high = 99.80. Probability/Score threshold: 0.6. Overlap threshold: 0.5. Output type: Labels only. Normalization axes: ZYX. Time-lapse labels: Match to previous frame (via overlap). Individual regions were extracted and cropped using square shape layers for each region. For each channel, the segmentation data was analyzed with RegionProps (napari-skimage-regionprops 0.10.1) to extract positions, size and signal intensity of each individually segmented cell and exported to a data table. The number and ratio of cells for each region was plotted using ggplot2. Density plots were made using the ggplot2 geom_bin2d option, using 15 bins. For each region, using centroid data, the x/y coordinates were scaled between 0-1, where 0 was the minimum pixel position where the first cell was along the x/y axis, and 1 the maximum position where the last cell was along the x/y axis, to account for small variations in size and crops, to better capture the average pattern.

Live cell micropattern imaging

For live cell imaging and tracking of different co-cultured mESC lines, the pSLQ1371 sgRNA plasmid was modified by replacing mCherry for either Clover or mTagBFP. The Myc nuclear localization signal (NLS) was also added to the C-terminus each fluorescent protein (mCherry-NLS, Clover-NLS and mTagBFP-NLS). The mESC line with stably integrated inducible dCas9-VPR was transduced

via lentivirus with DNA encoding for either sgCtrl-mTagBFP-NLS, sgGata6-mCherry-NLS, or sgCtrl-Clover-NLS, as described before.

For live cell micropattern culture, RosetteArray™ (Neurosetta, Spinal 6-Well 100μm RosetteArray™ Plate) 6 well plates were used with 100 um growth regions. Wells were washed once with 1x PBS, followed by incubating 3 ml of 4 μg/ml Laminin in 1x PBS for 6 hours in a cell culture incubator for 6 hours at 37°C, 5% CO2. Wells were washed once with 3 ml 1x PBS per well one well at a time. Then, one well at a time, complete solution was removed and 2 ml standard differentiation medium was added. Plates were placed in the incubator until needed the same day. sgCtrl-mTagBFP-NLS-mESCs, sgGata6-mCherry-NLS-mESCs and sgCdx2-Clover-NLS-mESCs were individually collected, counted, and mixed together in a 1:1:1 ratio. Then, 400,000 cells were added per well (133,000 for each line) in a volume of 1 ml, so the total volume per well was 3 ml. After 6 hours, doxycycline was added to treatment wells. Medium was changed daily, one well at a time. For live cell imaging, the plate was placed in a Lionheart FX imager equipped with a humidity chamber, temperature (37°C) and CO2 (5%) control. Cells were imaged every hour for 48 hours total, using phase contrast, YFP and TexasRed channels.

Live cell micropattern image segmentation and processing

Tiled images obtained by Lionheart FX were stitched using Gen5 3.14 software. Time-lapse data was imported into imageJ as image stacks and individual micropattern regions were cropped and saved as individual image sequences per channel. For each micropattern region, the time-lapse data was imported as stacks into Napari. Cells were segmented using StarDist with label over time option. Next, Btrack plugin (0.6.4) was used to track individual cells in timelapse data and exported as h5 files. Default Btrack "cell" settings were used, except Motion Accuracy was increased to 10. For videos of live cell data, layers were arranged and/or overlaid in Napari and exported using wizard plugin (napari-animation 0.0.7). For detailed analysis of cell dynamics, cell displacement data was extracted from h5 files into.csv file format and further processed using CelltrackR (1.1.0).[99] For division rate, cells that divided twice or more during the experiment were included, and time in hours between division was measured. Angles were calculated in reference to the center of each micropattern region between individual cell data points in the timelapse imaging data. Displacement was calculated by measuring the absolute difference between x-y positions per cell at each timepoint in their respective tracks. For distance from center, an x-y coordinate system was calculated from minimum and maximum x-y values for each region and cells were positioned accordingly at each time point using each individual cell x-y values.

CRISPRa-programmed embryo model culture and immunofluorescence staining

To grow and differentiate mESCs in 3D structures, cells were grown in 24 well AggreWell 400 plates (Stemcell Technologies, 34415). Each well was washed once with 1x PBS, followed by adding 0.5 ml of anti-adherence solution (Stemcell Technologies, 07010). Plates were centrifuged 5 minutes at 1,000 rcf and incubated 20 minutes at room temperature. Anti-adherence solution was removed and 1 ml 1x PBS was added to each well. Plates were kept at room temperature until seeding cells. Just before seeding, 1x PBS was removed and 1 ml of standard differentiation medium + 20 uM ROCK inhibitor was added. To treatment wells, 1 μg/ml doxycycline was added. sgCtrl-mESCs, sgGata6-mESCs and sgCdx2-mESCs were individually collected, counted, and mixed together in a 1:1:3 ratio. Then, 32,000 cells were added per well (6,000 sgCtrl, 6,000 sgGata6 and 20,000 sgCdx2) in a volume of 1 ml, so that the total volume per well was 2 ml, and the final concentration of ROCKi was 20 uM and doxycycline was 0.5 μg/ml. After 24 hours, 1.4 ml of medium per well was replaced using standard differentiation medium without ROCKi, and repeated once. After another 24 hours 1.4 ml of medium was replaced per well. Doxycycline was added every medium change for treatment conditions. For conditions with altered cell ratios, the amount of cells was adjusted accordingly. For conditions with pre-induction of trophoblast lineages, sgCdx2-mESCs or sgCdx2+sgElf5 mESCs, cells were prepared 2 days prior to assembly of CPEMs, on gelatin coated plates at a seeding density of 9,000 cells / cm2 in 6 well plates. Cells were seeded in standard differentiation medium + 0.5 μg/ml dox, which was replaced with fresh standard differentiation medium + 0.5 μg/ml dox the next day.

After 72 hours in culture, CMEMs were prepared for immunostaining. 1.5 ml of medium was removed per well, and 1.5 ml of 1x PBS was added. CPEMs were allowed to settle for 1 minute, then 1.5 ml of this solution was removed for each well. 0.5 ml of 1x PBS was added per well. By tapping the plate and/or pipetting up and down, using a cut-off P1000 tip to prevent shearing, CPEMs were suspended and then transferred to 6 well plates already containing 2 ml of 1x PBS. A 40 um cell strainer (Corning, 087711), with the side tab cut off, was added to each well, so it forms a barrier to prevent update of CPEMs when aspiring solutions from the well. Alternatively, 74 um Netwell Inserts (Corning, 3477) were used in 12 well plates, in which all the volumes used were halved. For aspirating solutions, the plate was tilted slightly leading to approximately 0.5 to 1 ml of solution remaining to keep CPEMs in suspension. This way, 1x PBS was removed and each well was washed 2 ml of 3.6% formaldehyde in 1x PBS, followed by adding 2 ml of 3.6% formaldehyde in 1x PBS per well and incubated for 40 minutes at room temperature on an orbital shaker. For incubations, cell strainers were removed for improved mixing of CPEMs and buffers. During washes, cell strainers were briefly removed and reinserted after adding each wash to promote mixing of solutions. Formaldehyde solution was aspirated, then washed once with 1x PBS + 0.01% Tween + 1x Glycine (Cell Signaling Technology, #7005), and washed three times with 1x PBS + 0.01% Tween. Wells were washed twice with 1x PBS + 0.2% Triton-X100, followed by adding 2 ml of 1x PBS + 0.2 % Triton X-100 and incubated for 30 minutes at room temperature on an orbital shaker. Solution was removed and washed twice with Blocking buffer (1x PBS + 3% BSA + 0.1% Triton-X100), followed by addition of 2 ml Blocking buffer and incubated for 2-4 hours at room temperature on an orbital shaker. Solution was removed and washed twice with Antibody incubation buffer (1x PBS + 3% BSA), followed by addition of 2 ml of Primary antibody incubation solution per dish containing 1-2 μg/ml antibody each (Table S3). Dishes were incubated overnight at 4°C on an

orbital shaker. Primary antibody solution was removed and wells were washed four times with 1x PBS + 0.1% Tween. Wells were washed twice with an antibody incubation buffer (1x PBS + 3% BSA), followed by addition of 2 ml of Secondary antibody incubation solution per dish (Table S3). Dishes were incubated overnight at 4°C on an orbital shaker. Secondary antibody solution was removed and wells were washed three times with 1x PBS + 0.1% Tween. 2ml of DAPI incubation solution was added per well, consisting of 1x PBS + 0.01% Tween + 2 μg/ml DAPI, and incubated for 15 minutes at room temperature on an orbital shaker. Wells were washed twice with 1x PBS, then 2 ml of 1x PBS + 0.1 sodium azide was added for storage.

For imaging, CPEMs were transferred to glass bottom 8 well chamber slides (Ibidi, 80827). 250 μl of 1x PBS + 90% glycerol (Millipore Sigma, G2025) + 0.1% sodium azide was added to each well of the 8 well chamber slide. The 6 well plate containing CPEMs was slowly swirled so CPEMs cluster in the center and 50 μl was aspirated and added into the 8 well chamber slide wells. The lid was put on the 8 well chamber slide and sealed with clear nail polish (Ted Pella,114-7). Slides were stored overnight at 4°C to let the CPEMs settle before imaging. CPEMs were imaged on a Zeiss 880 confocal, using a 20x long working distance objective. For optical sectioning in the z-axis, images were taken every 3.89 um. The Oxford Instruments Andor BC-43 was used for CPEM imaging using a 20x objective.

CPEM image segmentation and processing for 3D analysis

Full image z-stacks were loaded into imageJ, and individual CPEMs were cropped from each image stack and saved as separate image sequences per channel. Image sequences per channel imported into Napari for each CPEMs and segmented using StarDist (stardist-napari 2022.12.6). The following settings were used: Model Type: 2D. Pre-trained model: Versatile (fluorescent nuclei). Normalize image yes, percentile low = 1.00, percentile high = 99.80. Probability/Score threshold: 0.6. Overlap threshold: 0.5. Output type: Labels only. Normalization axes: ZYX. Time-lapse labels: Match to previous frame (via overlap). Remaining parts of other CPEMs in the segmentation label layers were erased, so only data for a single complete CPEM was analyzed. For each channel, the segmentation data was analyzed with RegionProps (napari-skimage-regionprops 0.10.1) to extract positions, size and signal intensity of each individually segmented cell and exported to a data table. Data was filtered with the following parameters: Nuclei with mean intensities >400 (Pou5f1), >200 (Cdx2, Foxa1/2) were included in downstream analysis. Nuclei with areas >400 <16000 were included in downstream analysis. The number and ratio of cells for each region was plotted using ggplot2. Density plots were made using the ggplot2 geom_bin2d option, using 9 bins. For each region, using centroid data, the x/y coordinates were scaled between 0-1, where 0 was the minimum pixel position where the first cell was along the x/y axis, and 1 the maximum position where the last cell was along the x/y axis. In the z-axis, using centroid data, the z-position was normalized to the first image in which cells were detected for each sample. This accounted for small variations in size and crops of CPEM data, and the position in the imaging buffer during acquisition, to better capture the average pattern. Cavity analysis was done in imageJ,[100] by plotting the line intensity profile across a center-stack image of DAPI channel per sample. Plotting and clustering was done using PlotTwist.[101]

CPEM image processing for comparing trophoblast cell differentiation methods

Center z-stack images from sgCdx2, sgCdx2+sgElf5, pre-induced and non-pre-induced were loaded into imageJ and individual CPEMs were cropped from each image and saved as separate files per channel. Files were loaded as a stack in Napari and segmented using StarDist as described before, except the Time-lapse labels were changed to "unique through time" to apply unique labels per image. Segmentation was analyzed again using RegionProps. Cell ratios per CPEM were calculated based on the output and plotted using ggplot2. To assess Pou5f1 levels in Cdx2 segmented cells in each condition, the Cdx2 segmentation labels were instead used to measure the Pou5f1 channel and used to plot the Pou5f1 intensity.

CPEMs with an equal or above ratio of 0.1 were assigned as having a sufficient TS compartment. To analyze regional localization of Cdx2+ cells, center z-stack images were imported in ImageJ and the intensity profiles of Pou5f1 and Cdx2 stainings were measured along the inner compartment of CPEMs (Figure S6E). The measurements over the measurement length were binned into 20 intervals per CPEM, containing the average signal per channel per bin. Data was plotted and clustered using the PlotTwist app.

CPEM image processing for quantification of AVE related markers

CPEM z-stack images were loaded in ImageJ and individual CPEMs were cropped from each image and saved as separate files with the same dimensions. CPEMs were prepared for immunostaining and imaged as described before. Coordinates of Cer1, Dkk1 and Lefty1 positive labeling were measured per CPEM. To quantify Cer1, Dkk1 and Lefty1 staining measurements, images were divided into 4 quadrants using an X-Y coordinate system. The number of positive staining labels were counted and assigned to a quadrant based on their position. Only CPEMs with 2 or more labels per staining were included in quadrant analysis. CPEMs with 2 day pre-induced sgCdx2 mESCs were used in these experiments.

Analysis of basement membrane in CPEMs and CRISPRa perturbations

CPEMs were grown as described before, with 2 day pre-induced sgCdx2-mESCs. Additionally, sgCtrl-mESCs were replaced with either sgLama1-mESCs, or an equal combination of sgMmp2- and sgMmp14-mESCs. CPEMs were prepared for immunostaining and imaged as described before. Center z-stack images from CPEMs were loaded in ImageJ and individual CPEMs were cropped from each image and saved as separate files. To measure basement membrane integrity based on laminin alpha 1 (Lama1) antibody staining, images were thresholded in the Lama1 channel to create a binary signal for Lama1 positive and negative regions. The laminin binary mask was measured by measuring along a line following the basement membrane per CPEM. A gap was determined as a

Please cite this article in press as: Lodewijk et al., Self-organization of mouse embryonic stem cells into reproducible pre-gastrulation embryo models via CRISPRa programming, Cell Stem Cell (2025), https://doi.org/10.1016/j.stem.2025.02.015

minimum of 2 continuous pixels negative for Lama1 staining. The number of gaps was normalized to the length of the basement membrane per CPEM. To compare between Epi and Non-Epi compartments, two separate measurements were done along these regions. To measure thickness, the images were also thresholded in the Lama1 channel and the area of the thresholded Lama1 staining along the basement membrane was measured. Thickness was calculated by dividing the area by the length. These measurements were done separately for Epi and Non-Epi domains as indicated. Axis difference was used as a measure of elongation, per CPEM, in the center z-stack image, the longest and shortest axis was measured. The difference between axes was calculated and normalized to overall CPEM size.

CPEM scRNA-seq sample preparation

CPEMs were grown as described before for 72 hours. 1.5 ml of medium was removed and 1.5 ml of 1x PBS was added per well. 1.5 ml of this solution was removed and 0.5 ml of 1x PBS was added per well and CPEMs were transferred to microcentrifuge tubes using cut-off pipette tips. Tubes were centrifuged for 5 minutes at 300 rcf. Supernatant was removed and CPEMs were gently resuspended in 1ml of DMEM/F12 (Thermo Fisher, 11039021), followed by centrifugation for 5 minutes at 300 rcf again. Supernatant was removed and CPEMs were resuspended in 1 ml of Trypsin-EDTA. CPEMs were pipetted up and down 3 times before incubating for 5 minutes at 37°C. CPEMs were pipetted up and down 6 times and 200 μl of ESC qualified FBS was added to each tube, followed by centrifugation for 5 minutes at 300 rcf. Supernatant was removed and cells were resuspended in 0.5 ml standard differentiation medium and transferred to a cryovial. A sample was taken to measure cell viability, samples with viability >80% were used for downstream application. 0.5 ml of 2x Freezing medium, consisting of 85% ESC qualified FBS / 15% DMSO, was added to each cryovial and gently mixed. Cryovials were placed into a cell freezing container and incubated at -80°C overnight, followed by storage in liquid nitrogen (vapor phase) cell storage before single-cell RNAseq preparation. Approximately 1 million cells were frozen per cryovial. An additional vial was frozen from the same batch of CPEMs for each sample. This additional vial was thawed and assessed for cell viability again, before preparing for single-cell RNA-sequencing.

Cryovials were delivered for processing to Novogene Co, San Jose, USA, where samples were prepared following 10X Genomics v3 single-cell 3' RNA-seq library preparation. 4 samples were prepared, 5,000 cells were captured for each, and parallel sequenced (NovaSeq 6000) with 200M paired read output per sample, resulting in approximately 40,000 paired reads per cell per sample.

scRNA-seq analysis

Fastq files were aligned and gene counts and barcodes were processed using kallisto-bustools[102] kb_python-0.28.2.

The resulting output matrices were filtered and converted to seurat files (Seurat 5.0.1)[103] to perform data normalization and clustering. The seurat files were used to prepare umap plots, featureplots and dotplots shown.

The seurat for the mixed cell CPEM sample was also used for ligand-receptor interactions using CellChat v2 (2.1.1).[65]

Comparative scRNA-seq data analysis

To compare CPEM scRNA-seq data with mouse embryo data, canonical correlation analysis (CCA) was done using Seurat. Raw CPEM and mouse embryo single cell expression matrices were processed with the same parameters as described before for CPEM data analysis. To run the correlation analysis, the RunCCA option was using the CPEM and mouse embryo objects as inputs. For analyzing clusters in CPEM and mouse embryo data after CCA, the FindTransferAnchors option was used with the mouse embryo data as reference and the CPEM data as query. Predicted mouse embryo cell types in CPEM data were then calculated using the TransferData option and assigned their respective cell types from the mouse embryo annotation.

To compare the CPEM, ETX and mouse embryo cell cluster gene expression profiles in more detail, the ClusterFoldSimilarity package was used.[62] Similarity tables and matrices were generated in pairwise comparisons between possible combinations of the datasets.

For pseudo-bulk analysis of Cdx2 expression in CPEM scRNA-seq data, the average gene expression was calculated for Cdx2 expressing cells per cluster, using the CPEM-Mix and sgCdx2-only scRNA-seq from this study. This was compared with bulk 3'UTR RNA sequencing of mESCs with Cdx2 cDNA induction time-course data and established TSC line data.[2] Eif1 was used as a reference gene to calculate relative expression between datasets, as it showed stable expression across conditions and cell lines.

QUANTIFICATION AND STATISTICAL ANALYSIS

Software used and methods for analysis and quantification of each data type in this manuscript are described in the method details section.

Figure legends show the number and type of replicates used for the represented data, as well as precision measures. Statistical testing in Figure 7 was done using two-tailed unpaired student's t-test (microsoft excel) to measure statistical significance ($p < 0.05$).